Master's thesis

NTNU
Norwegian University of Science and Technology
Faculty of Engineering
Department of Marine Technology

Benoit de Renty

Gradient-based design optimization of a semi-submersible floating wind turbine

Master's thesis in Marine Structures
Supervisor: Erin Bachynski
July 2020

NTNU
Kunnskap for en bedre verden

Benoit de Renty

Gradient-based design optimization of a semi-submersible floating wind turbine

Master's thesis in Marine Structures
Supervisor: Erin Bachynski
July 2020

Norwegian University of Science and Technology
Faculty of Engineering
Department of Marine Technology

NTNU
Norwegian University of
Science and Technology

Master thesis

Gradient-based design optimization of a semi-submersible floating wind turbine

---

Benoit de Renty

Department of Marine Technology
NTNU
Spring 2020
Supervisor: Erin Bachynski

Abstract

This work presents a linearized model of a floating wind turbine using the semi-submersible OOStar base geometry, a 10MW turbine and automation of the potential flow coefficients computation. It is associated with a design optimization problem which minimizes the cost of the platform w.r.t. two hull-shape geometric variables. Constraints based on international standards, limiting the maximum motion, stress and fatigue response are applied. A comparison with state-of-the-art non linear simulations showed that the response to waves is rather accurate but the response to wind needs to be improved for above-rated wind speeds. The linear model is however acceptable for capturing trends in the system's dynamics and is therefore suited for early design stage calculation. Eventually, the model is used to explore the design space manually, and identify optimization trends. The decrease in the columns' diameter is limited by the resulting drop in pitch restoring and by the pitch natural frequency getting too close to the wind excitation range. Decreasing the pontoon length drives the heave frequency dangerously close to the wave frequencies.

Acknowledgments

I would like to express my gratitude to my supervisor Erin Bachynski for the guidance, help and patience that she gave me throughout this project, but also for the great lectures that she conducts at Marintek. I would like to thank John Marius Hegseth for taking the time to answer every single one of my questions. Finally, I need to thank my favorite French duo, Tom & Bapt, whose love for adventure, good food and bad jokes made this year memorable.

Table of contents

List of Figures

List of Tables

NTNU Trondheim
Norwegian University of Science and Technology
Department of Marine Technology – Group of Marine Structures

PROJECT THESIS IN MARINE TECHNOLOGY

SPRING 2020

FOR

STUD.TECHN. Benoit de Renty

Gradient-based optimization of large-volume floating wind turbines
Gradient-basert optimering av storvolum flyttende vindturbiner

Background:
The offshore wind industry is moving toward deeper water, farther from land, where floating wind turbines (FWTs) become more economical than bottom-fixed turbines. The costs of FWTs still far exceed their bottom-fixed counterparts, and researchers are actively searching for opportunities for cost reduction. More efficient design of the substructure is seen as a possible method to bring costs down.

Multidisciplinary design optimization techniques – where (for example) the substructure geometry, tower design, wind turbine control parameters, and mooring system are optimized simultaneously – can provide novel designs which can reduce costs. A simplified frequency-domain model for use in optimization has been developed, but it is currently limited to spar-type wind turbines where the hydrodynamic properties can be easily estimated. In order to allow for more generic shapes, the method needs to be extended to include solving the potential flow problem for the defined hull form. Furthermore, calculation of the gradients with respect to the potential flow solution must be addressed.

Assignment:
The following tasks should be addressed in the project work:

1. Literature review regarding floating offshore wind turbine concepts and dynamic modelling, multidisciplinary design optimization, and potential flow theory.

2. Familiarization with the linearized analysis model from John Marius Hegseth, and implementation of a (rigid hull) semi-submersible (OO Star). This may require modification of the code.

3. Comparison between linearized results and SIMA analysis for the OO Star model.

4. Automation of the generation of potential flow coefficients using WAMIT or Genie/HydroD, considering only one or two possible geometrical modifications.

5. MDO in OpenMDAO using the linearized model and a finite differences approximation of the potential flow coefficient derivatives.

6. Report and conclude on the investigation.

The work scope could be larger than anticipated. Subject to approval from the supervisor, topics may be deleted from the list above or reduced in extent.

In the project, the candidate shall present his personal contribution to the resolution of problem within the scope of the project work.

Theories and conclusions should be based on mathematical derivations and/or logic reasoning identifying the various steps in the deduction.

The candidate should utilize the existing possibilities for obtaining relevant literature.

The project report should be organized in a rational manner to give a clear exposition of results, assessments, and conclusions. The text should be brief and to the point, with a clear language. Telegraphic language should be avoided.

The project report shall contain the following elements: A text defining the scope, preface, list of contents, main body of the project report, conclusions with recommendations for further work, list of symbols and acronyms, reference and (optional) appendices. All figures, tables and equations shall be numerated.

The supervisor may require that the candidate, in an early stage of the work, present a written plan for the completion of the work. The plan should include a budget for the use of computer and laboratory resources that will be charged to the department. Overruns shall be reported to the supervisor.

The original contribution of the candidate and material taken from other sources shall be clearly defined. Work from other sources shall be properly referenced using an acknowledged referencing system.

Erin Bachynski
Supervisor

Deadline: 06.06.2020

Introduction

In a world highly threatened by the consequences of climate change, and largely dependent on depleting resources, the need of transitioning to non-emitting and renewable sources of energy could not be greater. Developing offshore wind could be an effort in that direction, provided that politics and operators in the sector fully understand the challenges of such an intermittent source of energy, requiring expensive and resource-hungry manufacturing and installation.
Extracting the wind power away from the shore has already met its developers and a number of commercial offshore wind farms have been producing energy in the past years. But the desire to take advantage of stronger and more constant winds led to the design of floating platforms capable of supporting turbines in deeper waters and thus even further from land. As floating offshore wind becomes a more and more mature technology, it has been shown that scaling up the turbines is a way of reducing the levelized cost of energy (LCOE) of floating wind turbines (FWT). While the few floating concepts that are operating out in the sea currently don't exceed 6MW of rated power, the industry and the research are already looking at 10MW turbines as the future of offshore wind. In practice, this would mean larger substructures, possibly higher loads and definitely important challenges in terms of manufacturing and installation. With the substructure usually representing 15-30% of a FWT CAPEX, developing cheaper platform designs would have a significant impact on the overall system cost.

That's why numerical design optimization is extensively used for marine structures as it represents an efficient way of coming up with performant and cost-efficient designs. Clauss and Birk [1] made an early attempt of large-volume offshore structures optimization. The target was seakeeping and the objective to minimize was the significant amplitude of the overturning moment calculated on a design sea spectrum. They eventually managed to significantly reduce forces and motions on multiple structures by optimizing their shape and using long-term wave statistics. Still in the hydrodynamic performance, Park et al. [2] present a fully automated procedure for hull-form optimization of a semi-submersible floating production unit. The cost function is a weighted sum of the 3-hour heave most probable extreme value and the structural weight. The use of a simulated annealing algorithm (probabilistic) led to four optimized results, depending on the objective weight distribution.
Closer to our scope, research focused on offshore wind turbines optimization. In Karimi et al. [3], the design space includes the three stability classes of FWT. Two objective functions, the platform cost and the nacelle acceleration were minimized with a genetic algorithm. Evaluation and comparison of different platforms were performed using a Pareto front. In Chew et al. [4], the mass of a jacket supporting a 5MW turbine was minimized using an analytical gradient-based algorithm. A sequential quadratic programming (SQP) optimizer used the analytical direct differentiation method (DDM) to compute the gradients of the objective function and the constraints. Very few FWT design optimization were performed with a gradient-based algorithm. One of them comes from Fylling and Berthelsen [5], who minimized the cost of a spar buoy, its mooring and power cables using finite-difference method to calculate the gradients of the objective and the constraints. This introduces the complexity but also the great increase in efficiency that comes with computing analytical derivatives.
FWT are highly coupled systems, usually requiring hydro-aero-servo-elastic solvers to capture accurately the response to environments. Optimizing the platform, the turbine or the mooring separately would lead to a sub-optimal solution. Therefore it is desirable to use multidisciplinary optimization (MDO) to design all the components simultaneously. Lemmer et al. [6] included a self-tuning controller in the floater geometric optimization of a semi-submersible mounted with a 10MW turbine. They managed to reduce the wind and wave loads at the expense of an increased material cost. An integrated optimization of spar-type FWTs has been done by Sandner et al. [7]. Two models of a varying level of detail were used to optimize both the hull and the control system at the same time. The cost function included the rotor speed and the tower bending degree of freedom instead of tower base moment, since no structural model was included. Ashuri et al. [8] also used a MDO architecture to perform an integrated aerodynamic and structural design of the rotor and tower of an offshore wind turbine simultaneously. The result of the design optimization process shows 2.3% decrease in the levelized cost of energy. Recently, a linearized aero-hydro-servo-elastic floating spar wind turbine model was developed by Hegseth et al. [9] to optimize simultaneously the platform, tower, mooring system, and blade-pitch controller. Using a gradient-based algorithm and analytical derivatives the optimization showed that the solutions for the tower and blade-pitch control system are clearly affected by

the simultaneous design of the platform. This integrated and efficient model is however limited to spar-type wind turbines, where the hydrodynamic properties can easily be estimated. Yet, the analysis of large-volume substructures like semi-submersibles ususally requires solving the potential flow problem.

The presented project aims at extending gradient-based optimization processes to semi-submersible substructures requiring the computation of frequency-dependent potential flow coefficients. This report develops a simplified model of a semi-submersible platform, inspired from the Olav Olsen's OOStar, topped with a 10MW turbine. It uses a potential flow solver to generate the hydrodynamic coefficients and computes the linearized response of the rigid-body platform and flexible tower in the frequency domain. The model is implemented in the OpenMDAO framework [10] to optimize the dimensions of the platform using a gradient-based algorithm. A function of the platform cost is minimized w.r.t two geometric parameters, while constraints regarding the stability of the system, fatigue and strength of the tower are applied. The purpose of the project is to see if the optimization can identify key parameters or trends for cost reduction, as well as driving constraints for the design of semi-submersibles. This work also aims at building a computationally efficient tool for early design stage, which allows the designer to quickly evaluate the consequence of a design change in the general behavior of the system.
The current report presents in section 1 some theoretical background about FWT, optimization and potential flow theory. The FWT model is described in section 2 and the optimization problem is detailed in section 3. In section 4, a training model was developed to practice with the OpenMDAO framework. Section 5 validates the linear results and apply the model to several points in the design space.

1 Theory

This section serves as a theoretical background for the major concepts used during the work. It gives some literature-based insights in the FWT technology, such as system dynamics, design and modeling. Since the model developed in the report uses potential flow hydrodynamic coefficients, some basic elements about this theory are given. Finally, this section provides an introduction to the vast topic of numerical optimization and gives more details about the specific optimizer used in this report.

1.1 Review of FWT technology

1.1.1 Basic concepts of FWT

Chapter 9 of Offshore Wind Power [11] details some of the design drivers for the floating substructures supporting wind turbines. Among the most important is resisting the steady component of the turbine thrust and therefore ensuring enough static stability. This can be achieved in several ways and leads to the different stability classes. Floating support structures for wind turbines can generally be classified in three main groups. Naturally, all the real platforms actually use a combination of these stability types, but they are mainly characterized by one of them. Butterfield et al. [12] help understanding the characteristics of these groups:

- The ballast-stabilized platforms use heavy weighting far down the platform to place the center of gravity way below the center of buoyancy. It thus creates a righting moment and ensures a high inertia resistance in roll and pitch. The draft is usually large. The projected area to the waves is relatively small and the natural frequencies are rejected below the wave frequencies, creating slow and small motions. Typical examples are spar platforms, like the Hywind spar developed by Equinor for the Hywind Scotland wind farm.
- The buoyancy-stabilized platforms use a large and/or distributed waterplane area to ensure large hydrostatic restoring. In return, they usually have a large projected area to waves yielding higher loads and important motions of the floater. This is the principle used by barges and to some extent by semi-submersibles, like the WindFloat concept developed by Principle Power and field-tested in Portugal.
- The mooring-stabilized platforms use mooring tension combined with excess buoyancy to reduce the motion response. Structures like tension-leg platforms (TLP) have high vertical stiffness and shift the natural frequencies above the wave frequencies. The result is small motion but a more challenging installation.

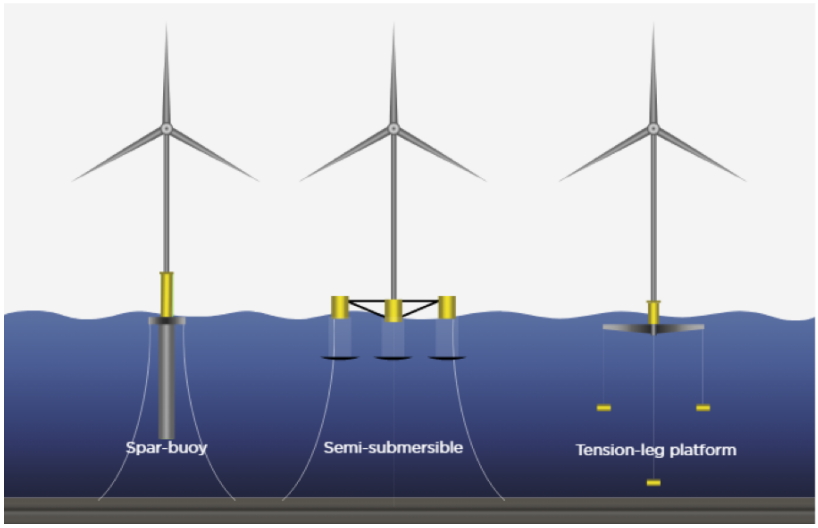

Figure 1: The three main concepts of floating support structures for offshore wind turbine

Robertson, Jonkman and Matha [13] [14] provide a thorough comparison of different platforms dynamics among the mentioned concepts. They found that the dynamic coupling between the turbine and the platform induced, for all the cases, increased loads in the turbine components compared to land-based. The turbines must therefore be strengthened to account for e.g. higher bending moment in the tower, at the blade root and at the yaw bearing. Moreover, two different designs belonging to the same stability class have pretty similar responses which means that the method for stabilizing the platform has greater impact on the system's dynamics than the design details. Finally, the TLPs, spars and semi-submersibles don't show significant difference in terms of fatigue and ultimate loads (except for the loads in tower which are lower for a TLP).

Another important design driver from is to minimize the motions due to the wave loads [11]. This can be achieved by reducing the area of the structure projected against the waves near the waterline. The main structure should consequently be above the highest wave or deeply submerged. Moreover, having natural frequencies away from the wave frequencies is essential to avoid resonance. Increasing the hull inertia also helps reducing the motions. Less conventional solutions are the use of damping plates or vortex-suppression strakes.

1.1.2 FWT design

LIFE50+ is an international collaborative project funded by European Horizon-2020 and led by SINTEF Ocean. It aims at "proving cost effective technology for floating substructures for 10MW wind turbines at water depths greater than 50m". The outcomes of the program are two mature floating substructure designs in line with 10MW-turbines ambitions, increased scientific and industrial knowledge on numerical and experimental design methodologies and procedures, and ultimately, a considerable LCOE reduction for large floating offshore wind farms. The resulting deliverables provide a very recent overview of the FWT state-of-the-art technology.

The report [15] uses a synthesis of the existing design practices to provide a state-of-the-art procedure for designing FWT substructures. In particular, figure 7 in the report presents a high-level design diagram. It gives reference procedures in every aspect of FWT design for the three main stages, "conceptual design", "basic design" and "detailed design". These three major steps typically involve calculations based on spreadsheets and frequency-domain models followed by coupled aero-hydro-servo-elastic time domain simulations, and finally component-specific analysis.
More in our interest, the part on the substructure design recalls the two methodologies for hydrodynamic analysis: computational models and more complex water tank test campaigns to validate the computational results as well as to calibrate the parameters used in the models.

1.1.3 FWT dynamics

A floating wind turbine dynamic response is mostly characterized by its natural frequencies. Hydrostatic restoring, mooring stiffness and mass properties create a natural frequency in the six degrees of freedom. The coupling between the tower and the support structure yields tower bending natural frequencies that are different from a stand-alone tower.

Jonkman et al. [13] conducted a dynamic numerical analysis of three platforms from the three stability classes. The results, partly described in figure 2, show how the dynamic response is typically spread across the frequencies. The DeepCWind model test campaign [16] provides experimental RAOs for the same concepts (Figure 3). The systems are designed such that most of the system modes don't lie in the wave-excitation region, so one can see that there is little response in the wave frequency range. Non linear effects can excite the systems at lower and higher frequencies and trigger resonant motions. At resonance, damping is essential to limit the response.

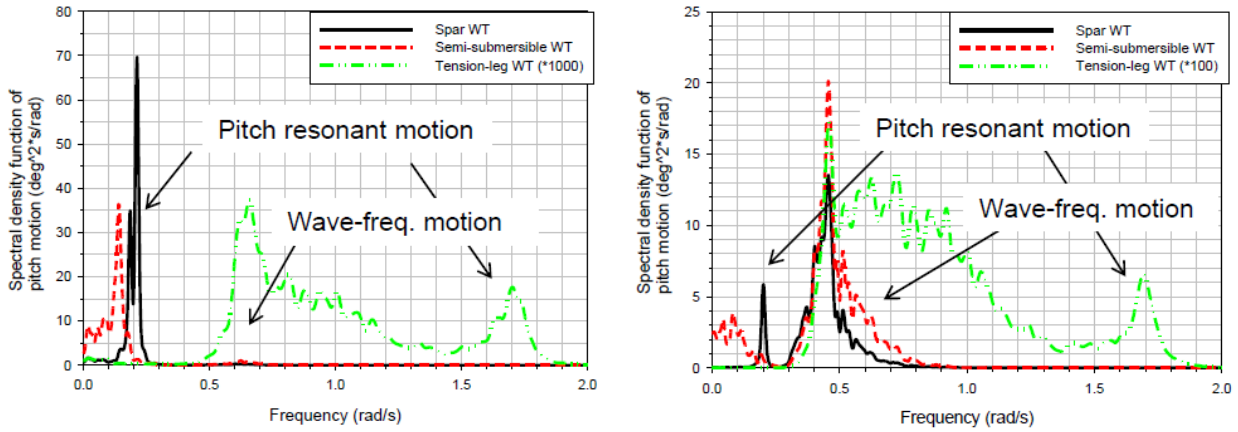

(a) Environmental condition : Uw=11.4 m/s, Hs=3.1 m, Tp=10.1 s

(b) Environmental condition : Uw=50 m/s, Hs=12.7 m, Tp=14.1 s

Figure 2: [17] Dynamic pitch response of three FWT concepts

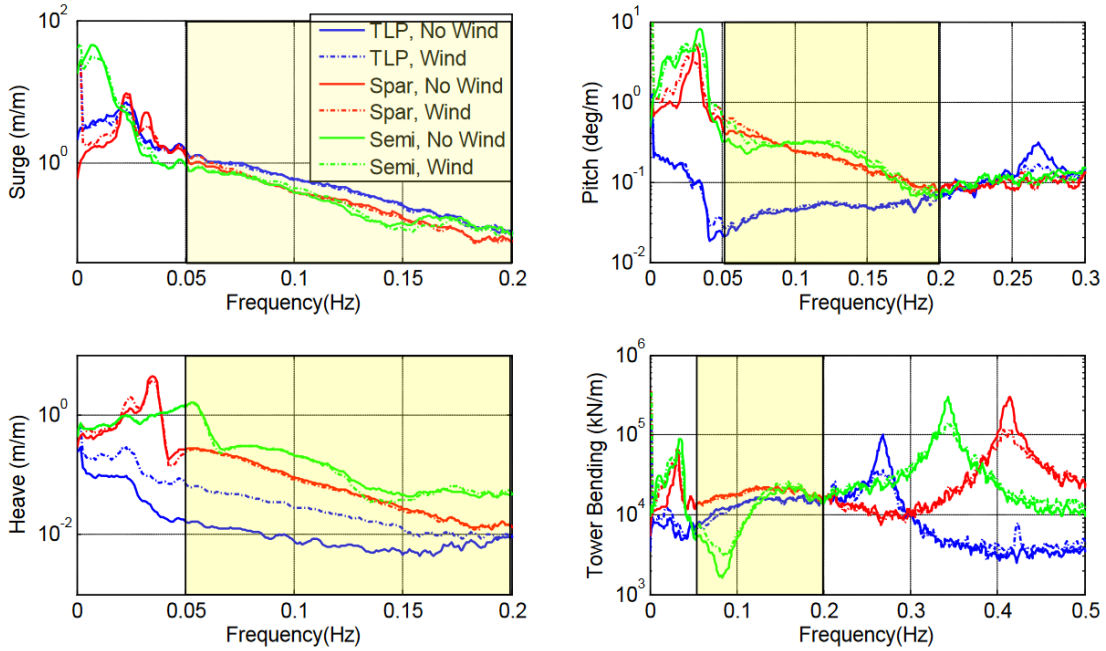

Figure 3: [16] Experimental RAOs derived from white-noise wave excitation with Hs=7.1 both with and without wind present at 21.8 m/s; colored box indicates wave frequency range

1.1.4 FWT numerical modeling

Floating wind turbines are highly complex systems. Figure 4 gives an idea of the numerous load and excitation sources on a FWT. Several aspects must be investigated when conducting at FWT analysis:

- Environmental conditions: the system is subject to turbulent wind fields and random waves
- Load analysis: forces resulting from environmental conditions result in aerodynamic loading on the turbine and hydrodynamic loading on the floater and the mooring.

- Response analysis: After integration of the loading, structural dynamics of the system and mooring response can be assessed
- Control theory: the turbine control aiming at optimizing the power production influences greatly the system's dynamics

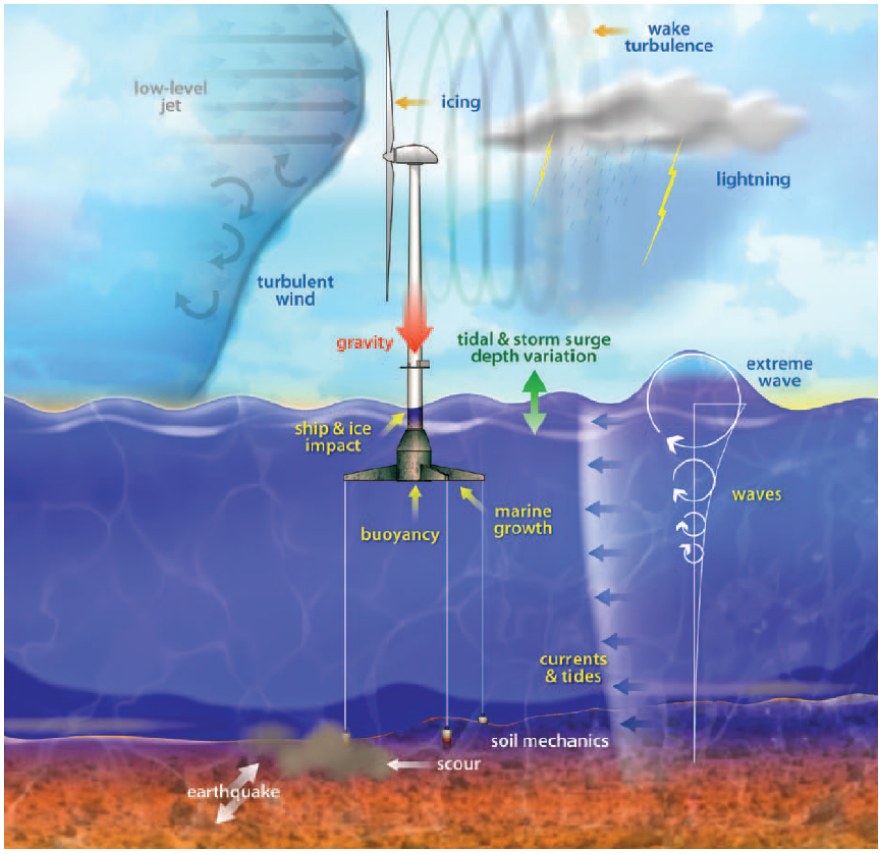

Figure 4: Load sources on a floating offshore wind turbine

In addition, non-linearities take place in the geometry (large blade deflection), in the loads (drag forces) and in boundary conditions (blade pitch actuator). The strong coupling between the aforementioned aspects and these non-linearities require integrated aero-hydro-servo-elastic time-domain simulations. [17] and [15] provide state-of-the-art modeling practice for aerodynamics, hydrodynamics and structures.

Hydrodynamic modeling:

For slender structures that are transparent to waves, Morison equation is used to compute inertia and drag forces. It is typically applied for bodies with a diameter D to wave-length λ ratio of less than $D/\lambda < 0.2$ and use added mass and drag coefficients from look-up tables or determined with experimental tests. In that case, the normal force on a moving structure in waves is given by equation 1. In long waves, $C_A = 1$ and the diffraction part of the excitation loads can be neglected, while in short waves, the diffraction is important. In small and moderate waves, the inertia force dominates, while in extreme waves, the drag force dominates.

$$f_N(t) = -\rho C_A A \ddot{r} + \rho\,(1 + C_A)\,Aa + \frac{1}{2}\rho C_D D v_r\,|v_r| \tag{1}$$

Where C_A and C_D are the added mass and drag coefficient, A is the cross-sectional area of the element, a is the water particle acceleration, $\ddot{r}$ is the body acceleration and $v_r = v - \dot{r}$ is the relative velocity between the water and the body.

For large-volume and hydrodynamically non-transparent structures, potential flow theory is used to solve

the diffraction-radiation problem. It is typically applied when $D/\lambda > 0.2$, for diffraction dominated cases. For first order potential flow theory, linear Airy wave theory is used for calculation of wave kinematics. The outputs are the frequency-dependent added mass and wave radiation damping matrices, as well as the wave excitation forces. Second order potential flow theory accounts for the sum and difference-frequency forces resulting from non-linearities of real surface waves. Higher order wave theories have to be applied depending on the wave height, period and water depth. With higher order potential flow theory, the instantaneous floater position and instantaneous water level can be applied. Finally, viscous effects are usually added using the drag term from the Morison equation.
More details into this theory are given in section 2.3.

Aerodynamic modeling:

The industry standard for wind turbine aerodynamics is the Blade Element Momentum theory. It combines the momentum conservation of a stream tube going through an actuator disk and the lift/drag forces on a 2D blade section. This computationally efficient method requires however corrections to account for local viscous effect, dynamic inflows, tip losses and tower shadow.

More advanced methods, based on potential flow , like the generalized dynamic wake method or the free vortex wake method can be used.

Structural modeling:

The whole turbine and the mooring is modeled with finite elements. Dynamic and non-linear FEM is needed to compute the stresses and deformation in the system. The floating platform is usually modeled as a rigid body.

1.1.5 Overall assessment of modeling practices on semi-submersibles

Robertson et al. [18] provide a synthetic comparison of the different codes used in the OC5 campaign to analyze their semi-submersible concept. The results showed that whatever theories were used in the integrated analysis, they all underpredicted the ultimate and fatigue loads compared to experiments. The regions with the largest underprediction of force were the low-frequency responses outside the wave-excitation region, associated with the excitation of the surge and pitch natural frequencies. Therefore, emphasis is laid on the importance of modeling non-linear forces, using second order potential flow theory or wave kinematics, wave stretching or application of the wave loads at the instant body position. For moorings, it was observed that having a dynamic (rather than quasistatic) model was important for capturing the ultimate and fatigue loads in the lines, and that the inclusion of hydrodynamic excitation from the waves could create larger line loads. For the hydrodynamics, the limitation of Morison equation to long waves is recalled, as well as the need to compute the dynamic pressure forces on the ends of the heave-plates when using Morison.
Kvittem et al. [19] also found that in the case of the WindFloat semi-submersible, Morison's equation compares well to potential flow theory if one chooses the coefficients carefully and integrates to the instantaneous free surface.

1.2 Optimization

In a pure mathematical point of view, optimization is the search for the optimum of a function within a domain defined by a set of variables and restricted by a number of constraints. It has been a field of interest in mathematics for centuries and has now been applied to many disciplines, among which is engineering.

An design optimization problem can be formulated in the following way:

$$\begin{array}{rll} \text{minimize} & f(x) & \\ \text{with respect to} & x \in \mathbb{R}^n & \\ \text{subject to} & \hat{c}_j(x) = 0, & j = 1, 2, \ldots, \hat{m} \\ & c_k(x) \geq 0, & k = 1, 2, \ldots, m \end{array} \tag{2}$$

f is the objective function
x is the vector of design variables
$\hat{c}$ is the vector of quality constraints
c is the vector of inequality constraints

The objective function is one measure of how "bad" a design is and can therefore be used to compare quantitatively different designs. The design variables are the ones changing along the optimization to eventually yield an optimal design. Constraints are limits that relate to practical design obligations, e.g. a marine structure must float and must not fail under certain environmental conditions.

Today, numerical optimization provides a way to automate the design process and to transition from finding a good or satisfying design to finding an optimal design. It has been extensively used in the marine world in order to improve structures design, performance or cost. The methodology usually assists the designer in the early design stages (i.e. conceptual design and basic design) to focus on the most feasible solutions from the beginning and thus speed up the overall design process.

A large number of optimization methods exist. They are usually divided between gradient-free and gradient-based methods. Gradient-free algorithms are the most widely used for marine structures, essentially because of their easier implementation. They allow a wide exploration of the design space but they usually can't give any optimality guarantee since they don't have access to derivative information. Their ambition is rather to find near-optimal points that are good enough for the given problem. Among them, the genetic algorithms and particle swarm method are suited for discrete variables and finding local minima. Gradient-free algorithms are quickly limited when the number of variables increases.

On the contrary, gradient-based optimizers are not exactly suited for a wide exploration of the design space. They are more valuable for a deterministic and systemic improvement of an existing design, where small changes actually make a difference. They perform way better than other methods when the number of design variables is large. However they are limited to smooth and continuous function. Their basic principle is to evaluate the gradient of the objective function and the constraints at every step to choose a "downhill" search direction. Gradient-based methods thus take a more direct path to the optimum. The resulting challenge is the calculation of the gradients, which can be computationally expensive and inaccurate if done with finite-difference, or tedious to implement if using analytical derivatives.

Numerous engineering problems are highly multidisciplinary. Designing a FWT, for example, requires analysis of structures, hydrodynamics, aerodynamics and control systems. It then sounds natural to optimize such a system by considering every aspect at the same time. This is seldom the case and optimization procedures usually converge towards sub-optimal solutions. Multidisciplinary design optimization techniques, where the substructure geometry, tower design, wind turbine control parameters, and mooring system are optimized simultaneously, can provide real novel optimized designs.

In parallel, simplified models of the structure to optimize is an essential part of the framework, as the numerous iterations that are part of an optimization procedure require a sufficiently small runtime. The LIFE50+ report on design practice for 10MW turbine support structures [20] outlines two innovation needs for future work. One is the need to develop more reliable simplified and cost-efficient numerical models to use in FWT optimization. The other one is a lack of a general optimization framework which provides precise procedures regarding the models and the optimizers.

The present work uses the well known gradient-based Sequential Quadratic Programming (SQP) algorithm to carry out the optimization. To understand its behavior, one needs to be familiar with the root finding Newton's method and the optimality conditions of constrained functions.

1.2.1 Optimality conditions

A local minimum of a smooth unconstrained function is usually defined where its gradient becomes zero and where its Hessian is positive definite.

In the case of a constrained function, optimal points are defined by the Karush-Kuhn-Tucker (KKT) conditions. These conditions are based on the Lagrangian function, which is defined as the objective function minus a weighted sum of the constraints.

$$\mathcal{L}(x, \hat{\lambda}, \lambda, s) = f(x) - \sum_{j=1}^{\hat{m}} \hat{\lambda}_j \hat{c}_j(x) - \sum_{k=1}^{m} \lambda_k \left(c_k(x) - s_k^2 \right)$$

$$\mathcal{L}(x, \hat{\lambda}, \lambda, s) = f(x) - \hat{\lambda}^T \hat{c}(x) - \lambda^T \left(c(x) - s^2 \right) \tag{3}$$

$\hat{\lambda}$ and λ are the vectors of the Lagrangian multipliers associated with respectively the equality constraints and the inequality constraints. s is a vector of slack variables. The idea here is to go from searching for the optimum of a constrained function to searching for the stationary points of an unconstrained function. One can see that a stationary point of the Lagrangian verifies the optimality condition on the function gradient and satisfies the constraints. A stationary point of the constrained function will satisfy the following:

$$\nabla_x \mathcal{L} = 0 \Rightarrow \frac{\partial \mathcal{L}}{\partial x_i} = \frac{\partial f}{\partial x_i} - \sum_{j=1}^{\widehat{m}} \hat{\lambda}_j \frac{\partial \hat{c}_j}{\partial x_i} - \sum_{k=1}^{m} \lambda_k \frac{\partial c_k}{\partial x_i} = 0, \quad (i = 1, 2, \ldots n) \tag{4}$$

$$\nabla_{\hat{\lambda}} \mathcal{L} = 0 \Rightarrow \frac{\partial \mathcal{L}}{\partial \hat{\lambda}_j} = \hat{c}_j = 0, \quad j = 1, \ldots, \widehat{m} \tag{5}$$

$$\nabla_{\lambda} \mathcal{L} = 0 \Rightarrow \frac{\partial \mathcal{L}}{\partial \lambda_k} = c_k - s_k^2, \quad k = 1, \ldots, m \tag{6}$$

$$\nabla_S \mathcal{L} = 0 \Rightarrow \frac{\partial \mathcal{L}}{\partial s_k} = \lambda_k s_k = 0, \quad k = 1, \ldots, m \tag{7}$$

$$\lambda_k \geq 0, \quad k = 1, \ldots, m \tag{8}$$

These are the first order "necessary" KKT conditions. They are not sufficient to guarantee a local minimum. A sufficient condition comes from second order information, on the Hessian of the function: the solution $x^*, \hat{\lambda}^*, \lambda^*$ and s^* found above is a constrained minimum if the Hessian at that point is positive definite in the subspace defined by the constraints. In other words, if

$$y^T \nabla^2_{xx} \mathcal{L} \left(x^*, \hat{\lambda}^*, \lambda^* \right) y > 0 \tag{9}$$

for any feasible direction y defined by

$$\nabla \hat{c}_j \left(x^* \right)^T y = 0 \quad j = 1, \ldots, \widehat{m}$$

$$\nabla c_k \left(x^* \right)^T y = 0 \quad \text{for all k for which } \lambda_k > 0$$

1.2.2 Newton's method

In optimization, Newton's method is an iterative process for minimizing a function using second order information. At each iteration, this method approximates the function with a second order Taylor expansion and finds the minimum of this quadratic approximation. It results in the construction of a sequence x_k that converges towards a minimizer x^*. At each iterate:

$$f(x_k + d_k) = f(x_k) + \nabla f(x_k)^T d_k + \frac{1}{1} d_k^T \nabla^2 f(x_k) d_k \tag{10}$$

The next iterate $x_{k+1} = x_k + d_k$ uses the minimum of this quadratic approximation. It is found by deriving the last expression w.r.t d_k and setting it to zero. The Newton step that minimizes the quadratic model therefore satisfies the following linear system:

$$\nabla^2 f(x_k) d_k = -\nabla f(x_k) \tag{11}$$

One can see that if f happens to be a quadratic function, the first iteration would directly find the optimum of f.

One limitation of this method is the computation of the second order derivative matrix, the Hessian $H = \nabla^2 f$, which can be quite challenging. Quasi-Newton methods were developed to approximate the function's Hessian based simply on first order information. The various quasi-Newton methods differ in how they update the approximate Hessian.

1.2.3 Sequential Quadratic Programming

The SQP method is the application of the Newton's method (or quasi-Newton) to the Lagrangian function defined previously. It takes Newton steps in the x and λ directions. If we consider a problem with only a set of equality constraints $\hat{c} = 0$, the Lagrangian function becomes $\mathcal{L}(x, \hat{\lambda}) = f(x) - \hat{\lambda}^\top \hat{c}(x)$. The Jacobian of the constraints is written $A(x) = \nabla \hat{c}(x)$ and the gradient of the objective function is written $g(x) = \nabla f(x)$. Applying Newton's method to the Lagrangian, the Newton step that minimizes the approximated quadratic model at point k is defined by:

$$\nabla^2 \mathcal{L}(x_k, \lambda_k) d_k = -\nabla \mathcal{L}(x_k, \lambda_k) \tag{12}$$

Detailing the coefficients of the Lagrangian's Hessian:

$$\nabla^2 \mathcal{L}(x_k) = \begin{bmatrix} \nabla^2_{xx} \mathcal{L}(x_k) & \nabla^2_{x\lambda} \mathcal{L}(x_k) \\ \nabla^2_{\lambda x} \mathcal{L}(x_k) & \nabla^2_{\lambda\lambda} \mathcal{L}(x_k) \end{bmatrix} = \begin{bmatrix} W(x_k) & -A(x_k)^\top \\ A(x_k) & 0 \end{bmatrix} \tag{13}$$

Inserted in the Newton equation, the Newton step is found as:

$$\begin{bmatrix} W(x_k) & -A(x_k)^\top \\ A(x_k) & 0 \end{bmatrix} \begin{bmatrix} p_{x_k} \\ p_{\lambda_k} \end{bmatrix} = \begin{bmatrix} \nabla f(x_k) - A(x_k)^\top \lambda \\ c(x_k) \end{bmatrix} \tag{14}$$

To account for inequality constraints, one of the most common types of strategy, the active set method, is to consider only the active constraints at a given iteration and treat those as equality constraints.

1.2.4 Computing derivatives

A major bottleneck in gradient-based optimization is the calculation of derivatives. We want them both accurate and efficient to have an effective optimization. Different numerical method of calculation are possible.

The finite difference method is very easy to implement and no source code is needed. It is however subject to potentially large errors and its cost is proportional to the number of variables. A first order Taylor expansion gives the expression:

$$f'(x) = \frac{f(x+h) - f(h)}{h} + \mathcal{O}(h) \tag{15}$$

It requires two function calls, which can be expensive is the considered function involves heavy calculation. The accuracy depends on the step size h. It should be small enough to have an accurate estimate of f', but not too small to avoid subtraction errors due to the finite number of digits that computers use to represent floats.

The complex step method gets rid of subtractive errors and improves the precision of the derivative estimate. However the function needs to support complex inputs and may therefore require some modification of the code.

$$f'(x) = \frac{\mathfrak{Im}[f(x+ih)]}{h} + \mathcal{O}(h^2) \tag{16}$$

Analytical methods are the most accurate and efficient ones. But they are tedious to implement as they require analytical expressions for the partial derivatives at every intermediate step in the model. They require detailed knowledge of the computational model but the cost is independent of the number of design variables. Typical methods are the direct and the adjoint method. In the end, analytical methods are the only hope for ambitious optimization with a large number of design variables.

1.3 Potential flow theory

Potential flow theory assumes non-viscous fluid and irrotational flow. The velocity in the fluid can then be expressed as the gradient of a potential function ϕ.

$$V(X,t) = \nabla\phi \tag{17}$$

This potential satisfies the Laplace equation in the whole fluid domain.

$$\nabla^2\phi = 0 \tag{18}$$

The velocity potential satisfies the boundary condition on the body surface, ensuring that the fluid velocity normal to the body is equal to the body velocity.

$$\frac{\partial\phi}{\partial n}(X,t) = \vec{V}(X,t)\cdot\vec{n} \tag{19}$$

and the non-linear free surface condition, ensuring the continuity in the pressure and the impermeability of the free surface

$$\frac{\partial^2\Phi}{\partial t^2} + g\frac{\partial\Phi}{\partial z} + 2\nabla\Phi\cdot\nabla\frac{\partial\Phi}{\partial t} + \frac{1}{2}\nabla\Phi\cdot\nabla(\nabla\Phi\cdot\nabla\Phi) = 0 \tag{20}$$

applied at the exact free surface

$$\zeta(x,y) = -\frac{1}{g}\left(\frac{\partial\Phi}{\partial t} + \frac{1}{2}\nabla\Phi\cdot\nabla\Phi\right)_{z=\zeta} \tag{21}$$

The pressure follows from Bernoulli's equation

$$p(X,t) = -\rho\left(\frac{\partial\Phi}{\partial t} + \frac{1}{2}\nabla\Phi\cdot\nabla\Phi + gz\right) \tag{22}$$

The velocity potential, the body motions and the wave elevation can be expanded in perturbation series

$$\begin{aligned}\Phi(\mathrm{x},t) &= \Phi^{(1)}(\mathrm{x},t) + \Phi^{(2)}(\mathrm{x},t) + \cdots\\ \xi &= \xi^{(1)} + \xi^{(2)} + \cdots\\ \zeta(x,y) &= \zeta^{(1)}(x,y) + \zeta^{(2)}(x,y) + \cdots\end{aligned}$$

Given a wave spectrum, it is usual to assume the spectrum is expressed as a linear superposition of the first-order incident waves of different frequencies. Thus the total first order potential for the wave-body interaction can be expressed by a sum of components having frequency ω_j:

$$\Phi^{(1)}(\mathrm{x},t) = \mathrm{Re}\sum_j \phi_j(\mathrm{x})e^{i\omega_j t} \tag{23}$$

At the second-order, the total velocity potential takes a form

$$\Phi^{(2)}(\mathrm{x},t) = \mathrm{Re}\sum_i\sum_j \phi^+_{ij}(\mathrm{x})e^{i(\omega_i+\omega_j)t} + \phi^-_{ij}(\mathrm{x})e^{i(\omega_i-\omega_j)t} \tag{24}$$

ϕ_{ij}^+ and ϕ_{ij}^- are referred to as the sum- and difference-frequency velocity potential with frequencies $\omega_i + \omega_j$ and $\omega_i - \omega_j$, respectively.

The induced forces are calculated by integrated the pressure on the body surface.

The first order wave-body interaction problem is obtained with the first order function components and by linearizing the boundary conditions. The problem is then divided in two sub-problems.

- In the diffraction problem, the body is assumed fixed. Incident waves, characterized by the velocity potential ϕ_I are diffracted on the body into scattering waves, characterized by the potential ϕ_S. The sum of the two potentials gives the diffraction potential ϕ_D. The resulting first-order excitation forces combine two contributions that can be separated theoretically but not physically: Froude-Krylov forces, induced by the unperturbed incident waves, and diffraction forces, induced by the perturbation alone.
- The radiation problem assumes an oscillating body in still water. Oscillation in every degree of freedom yields radiated waves with total velocity potential ϕ_R. The resulting forces present a component proportional to the body acceleration and a component proportional to the body velocity: $F_R^i(\omega) = -\sum_{j=1}^{N_{DoF}} \Big(A_{ij}(\omega)\ddot{X}_j(\omega) + B_{ij}(\omega)\dot{X}_j(\omega) \Big)$. The matrices A and B are the added mass and wave-radiation damping matrices.

The linearity of the problem allows the superposition of the two sub-problems, giving a total velocity potential:

$$\phi = \phi_I + \phi_S + \phi_R = \phi_D + \phi_R \tag{25}$$

Second-order wave forces also combine effects due to the incident wave and the diffracted wave. They are represented by their Quadratic Transfer Functions (QTF).

2 Floating wind turbine model

Since an optimization process involves several iterations to converge, it is necessary to use a simplified model to keep the computational time reasonable. The model that is developed in this work is therefore computationally-efficient but also low-fidelity. Its purpose is to quickly understand the system's basic characteristics, dynamic response and crucial performance like fatigue life and ultimate strength. It doesn't provide in-depth analysis of the system's performance, which would require non-linear coupled simulations.

The baseline design in the model is inspired from the Olav Olsen's OOStar semi-submersible. The main geometry is used, with a couple simplifications. First, the bottom skirt that surrounds the pontoons was removed. Second, the pontoons are not tapered and keep a constant width equal to the outer columns' bottom diameter. Without fundamentally changing the platform dynamics, these modifications simplify the geometry changes during the optimization. Other than that, the initial dimensions are the same as described in the public design definition report [21]. The hull geometry and the name of shape parameters are given in figure 6. The OOStar is described originally as a concrete platform but due to the lack of public information about internal structure of concrete hulls, a steel structure was preferred. More details are given in the mass model section. The turbine and the tower are also defined as in [21]. It's a modified version of the DTU 10MW [22] where the tower was adapted to withstand the semi-submersible dynamics. The mooring system is the one defined for the OOStar, three catenary lines connected to the top of the outer columns and divided in two segments by a clump weight.

The FWT is moored in open sea with 130m water depth. The model analyzes the response in the xz plane with aligned wind and wave in the x-direction. The model focuses only on three degrees of freedom, which are the rigid-body response in surge and pitch, and the first bending mode of the tower. It doesn't include any rotor model or controller. The only contribution from the rotor is a thrust force and aerodynamic damping. The equation of motion is linearized and solved in the frequency domain.

An integrated model of the OOStar and 10MW DTU turbine was built in the SIMA software, following the state of the art modeling of FWT. This high-fidelity model is used to provide the simplified optimization model with an accurate evaluation of constant characteristics of the system. The action of the wind on the rotor and the mooring stiffness are computed in that way. It is also used to compare and validate the performances predicted by the optimization model.

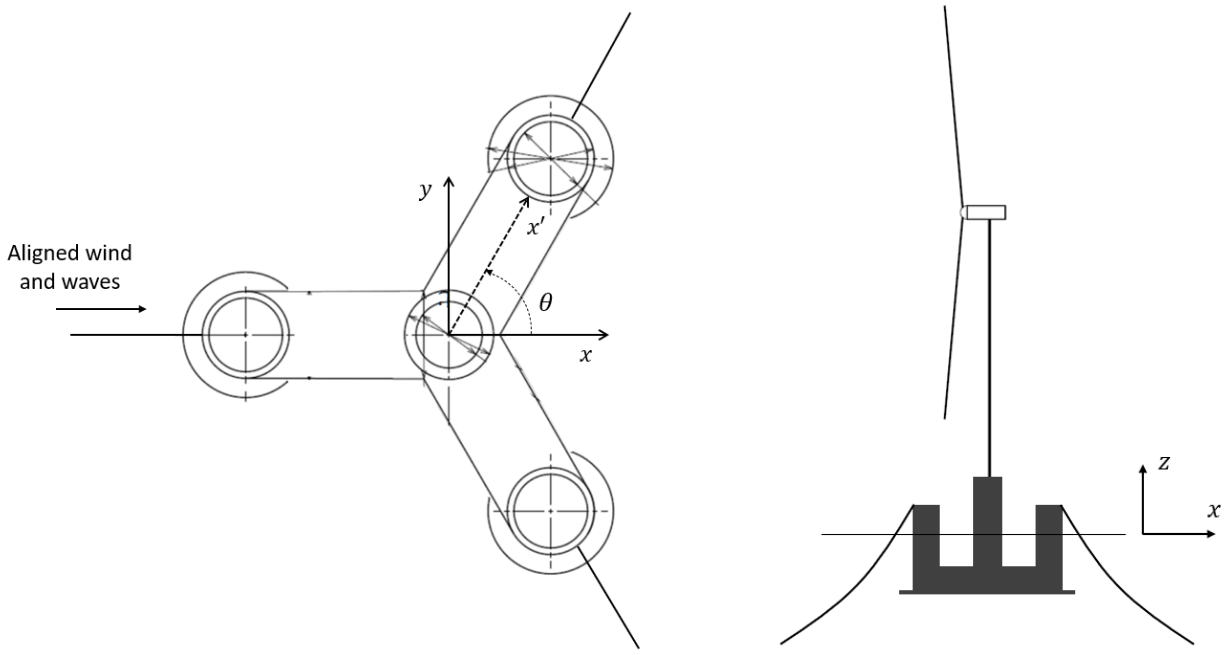

Figure 5: Description of the system

2.1 Mass model

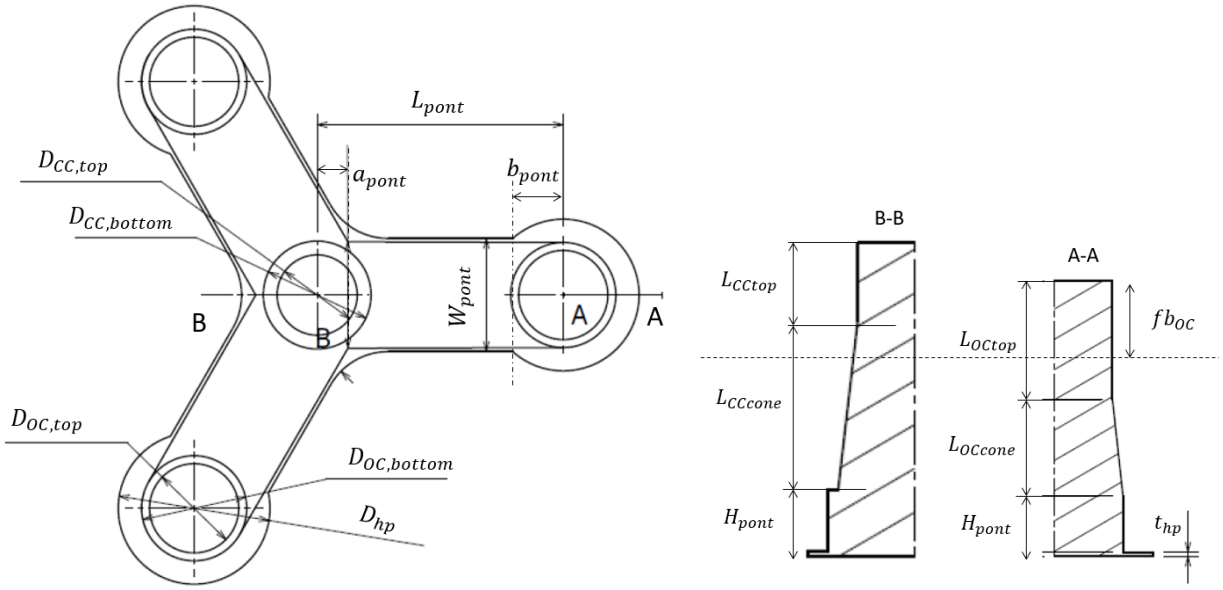

Figure 6: Parameterization of the platform

2.1.1 Steel mass distribution

As mentioned before, the OOStar is modeled here as a steel platform for simplicity. The hull doesn't present any prohibitive characteristic for being treated as a steel structure. The hull is therefore modeled as a hollow shell with steel walls of constant thickness t_w. For a braceless concept such as the OOStar, a steel mass M_{steel} equal to 0.23 times the displacement is a reasonable estimate [23]. Based on that estimate, the thickness of the outer shell t_w is calculated to be constant throughout the structure. The center of mass is approximated to be the center of volume of the hull.

To calculate the steel hull's pitch moment of inertia, the strategy is to divide the geometry into components of "standard shape", for which the inertia calculation is relatively easy. The inertia of each component is then expressed at its center of mass around local axis ($I_{x'}$, $I_{y'}$), displaced at the global origin around the global y-axis ($I_y(0)$) and added to the other moments of inertia. The mass of each considered component is written m and the angle between the global x axis and a pontoon is written θ.

Pontoons

The pontoon legs are assimilated as rectangular boxes, open at both ends, with length $L_{pont} - a_{pont}$, width W_{pont}, height H_{pont} and wall thickness t_w. The moment of inertia around the local longitudinal axis x' is

$$I_{x'} = \frac{m}{6}\left(W_{pont}^2 + H_{pont}^2\right)$$

The moment of inertia around the local transverse axis y' is found by integrating the parallel axis theorem applied to the 2D moment of inertia of a cross section.

$$I_{y'}^{2D} = \frac{\rho_s}{12}\left[W_{pont}H_{pont}^3 - (W_{pont} - 2t_w)(H_{pont} - 2t_w)^3\right]$$

$$I_{y'} = (L_{pont} - a_{pont})I_{y'}^{2D} + \frac{m}{12}(L_{pont} - a_{pont})^2$$

Finally, the pitch moment of inertia of a pontoon leg at the global origin is found as:

$$I_y(O) = I_{x'}\cos^2\theta + I_{y'}\sin^2\theta + m\left[\frac{1}{4}(L_{pont} + a_{pont})^2\cos^2\theta + (-draft + \frac{H_{pont}}{2})^2\right] \tag{26}$$

To complete the pontoons, the circular edges are modeled as hollow half cylinders with diameter D_{OCbot} and height H_{pont}. The moment of inertia around the local transverse axis x' and y' are equal to:

$$I_{x'} = I_{y'} = \frac{m}{12}\left[3(\frac{D_{OCbot}^2}{2} - D_{OCbot}t_w + t_w^2) + H_{pont}^2\right]$$

The pitch moment of inertia of the circular edges at the global origin is then:

$$I_y(O) = I_{x'}\cos^2\theta + I_{y'}\sin^2\theta + m\left[L_{pont}^2\cos^2\theta + (-draft + \frac{H_{pont}}{2})^2\right] \tag{27}$$

Outer columns

The outer columns' top part are hollow cylinders, open at both ends, with diameter D_{OCtop} and height L_{OCtop}.

$$I_{y'} = \frac{m}{12}\left[3(\frac{D_{OCbot}^2}{2} - D_{OCbot}t_w + t_w^2) + L_{OCtop}^2\right]$$

$$I_y(O) = I_{y'} + m\left[L_{pont}^2\cos^2\theta + (fb_{OC} - \frac{L_{OCtop}}{2})^2\right] \tag{28}$$

The OCs' cap are circular plates of thickness t_w.

$$I_{y'} = m\left[\frac{D_{OCtop}^2}{16} + \frac{t_w^2}{12}\right]$$

$$I_y(O) = I_{y'} + m\left[L_{pont}^2\cos^2\theta + fb_{OC}^2\right] \tag{29}$$

For the OCs conical part's moment of inertia, the formula for hollow cylinders, open at both ends, with diameter $D_{cone} = (D_{OCtop} + D_{OCbot})/2$ and height L_{OCcone} is used. However, the mass m and center of mass $Z_{g,cone}$ are kept as those of a cylinder.

$$I_{y'} = \frac{m}{12}\left[3(\frac{D_{OCcone}^2}{2} - D_{OCcone}t_w + t_w^2) + L_{OCcone}^2\right]$$

$$I_y(O) = I_{y'} + m\left[L_{pont}^2\cos^2\theta + Z_{g,cone}^2\right] \tag{30}$$

Central column

The same way as for the OCs, the pitch moment of inertia of the top part, cap and conical part of the CC are respectively:

$$I_y(O) = \frac{m}{12}\left[3(\frac{D_{CCbot}^2}{2} - D_{CCbot}t_w + t_w^2) + L_{CCtop}^2\right] + m\left[fb_{CC} - \frac{L_{CCtop}}{2}\right]^2 \tag{31}$$

$$I_y(O) = m\left[\frac{D_{CCtop}^2}{16} + \frac{t_w^2}{12}\right] + mfb_{CC}^2 \tag{32}$$

$$I_y(O) = \frac{m}{12}\left[3(\frac{D_{CCcone}^2}{2} - D_{CCcone}t_w + t_w^2) + L_{CCcone}^2\right] + mZ_{g,cone}^2 \tag{33}$$

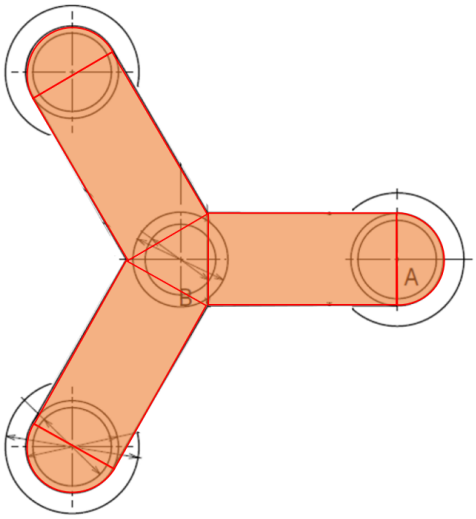

Figure 7: Description of the ballast distribution

2.1.2 Ballast mass distribution

Knowing the displacement, the steel mass, the tower mass and RNA mass, the ballast is calculated to have static equilibrium:

$$M_{ballast} = \nabla\rho - M_{steel} - M_{tower} - M_{RNA}$$

Figure 7 shows the ballast distribution in red: it is equally spread out in the pontoons, filled from the bottom up to a height $h_{ballast}$ to provide the correct mass. The ballasts are assumed to be solid blocks of concrete with density $\rho_{concrete} = 2600$ kg.m^{-3} . To calculate the moment of inertia of the ballast, the weights are divided into blocks in the same way as for the steel hull.

The pontoon legs are rectangular blocks of length $L_{pont} - a_{pont}$, width W_{pont} and height $h_{ballast}$. The local moments of inertia are:

$$I_{x'} = \frac{m}{12}\left(W_{pont}^2 + h_{ballast}^2\right)$$

$$I_{y'} = \frac{m}{12}\left((L_{pont} - a_{pont})^2 + h_{ballast}^2\right)$$

$$I_y(0) = I_{x'}\cos^2\theta + I_{y'}\sin^2\theta + m\left[\frac{1}{4}(L_{pont} + a_{pont})^2\cos^2\theta + (draft - \frac{h_{ballast}}{2})^2\right] \tag{34}$$

The end of the pontoons are half cylinders of diameter $D_{OC,bottom}$ and height $h_{ballast}$. For these blocks:

$$I_{x'} = I_{y'} = m\left(\frac{D_{OC,bottom}^2}{16} + \frac{h_{ballast}^2}{12}\right)$$

$$I_y(0) = I_{x'}\cos^2\theta + I_{y'}\sin^2\theta + m\left[L_{pont}^2\cos^2\theta + (draft - \frac{h_{ballast}}{2})^2\right] \tag{35}$$

The center block is a triangular prism of height $h_{ballast}$ and side W_{pont}:

$$I_y(0) = \frac{m}{12}\left(\frac{W_{pont}^2}{2} + h_{ballast}^2\right) + m\left(draft - \frac{h_{ballast}}{2}\right)^2 \tag{36}$$

2.2 Hydrodynamics

The studied platform has a large dimensions compared to the fluid motions in most sea states. The analysis of this type of platform is typically done with the potential flow theory. To account for viscous effects, additional damping is modeled with the viscous term of the Morison equation.

2.2.1 Potential flow

The hydrodynamic coefficients of the platform are calculated using the SESAM software package. The hull geometry is defined and meshed in GeniE to create an finite element model. Regarding the meshing, a rule of thumb is to have 6 elements per wavelength. If we take a broad estimation and consider that waves in open sea have a time period between 2s and 30s, in order to capture the smallest waves, the panels shall have a length of one meter. The FE model is then turned into a panel model in HydroD and the Wadam solver is called to solve the potential flow problem. We're interested here in the added mass, radiation damping and first order excitation forces in surge and pitch.

$$A = \begin{bmatrix} A_{11} & A_{15} \\ A_{51} & A_{55} \end{bmatrix} \qquad B = \begin{bmatrix} B_{11} & B_{15} \\ B_{51} & B_{55} \end{bmatrix} \qquad F_{\text{exc}} = \begin{bmatrix} F_{\text{exc},1} \\ F_{\text{exc},5} \end{bmatrix}$$

2.2.2 Viscous damping

The drag forces acting on the platform are modeled as an equivalent viscous damping matrix, formulated by a stochastic linearization of the Morison drag term [24]. This means that the drag force on a cylinder strip $dF_D = -\frac{1}{2}\rho C_D D u|u|$ is approximated by $dF_D = -\frac{1}{2}\rho C_D D\sqrt{\frac{8}{\pi}}\sigma_u u$. Here, σ_u is the standard deviation of the strip velocity. It is found using an iteration scheme and depends on the studied sea state. The excitation part of the drag forces is not taken into account as it is negligible in front of the potential excitation loads.

Figure 8 shows the drag elements of the structure: outer columns top and conical part in dark green and light green, central column in dark blue, pontoon circular edge in yellow, pontoon leg in blue and heave plate in red. The drag coefficient of every element is given in table 1 and is based on [25]. They are kept constant during the optimization. The linearized damping coefficients are obtained by considering the drag forces resulting from the surge and pitch rigid body motions of the platform η_1 and η_5. Each drag element is assigned a 2x2-sized B matrix, which, added together, form the linearized viscous damping matrix B_{visc}. This procedure is detailed hereafter. The notation $\tilde{C_D} = \frac{1}{2}\rho C_D\sqrt{\frac{8}{\pi}}$ will be used.

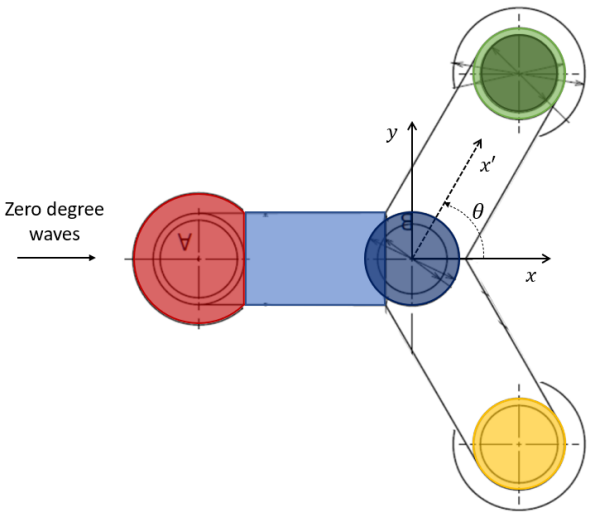

Figure 8: Drag elements of the structure

Outer columns

Considering first the outer columns top part, the horizontal velocity of a cylinder strip at depth z is $u = \dot{\eta_1} + z\dot{\eta_5}$. Therefore, the transverse drag force on this strip and the corresponding moment around $\vec{y}$ can be written:

$$dF_{D,1} = -\tilde{C_D} D \sigma_u \left(\dot{\eta_1} + z\dot{\eta_5}\right)$$
$$dF_{D,5} = z dF_{D,1}$$

The corresponding linear damping coefficients for one of the OC's top part are identified by integrating these elementary force and moment over the submerged part of the cylinder (from $d = -draft + H_{pont} + L_{OCcone}$ to the waterline).

$$F_{D,1} = -\int_d^0 \tilde{C_D} D \sigma_u dz \ \dot{\eta_1} - \int_d^0 \tilde{C_D} D \sigma_u z dz \ \dot{\eta_5} = -B_{11}\dot{\eta_1} - B_{15}\dot{\eta_5} \tag{37}$$

$$F_{D,5} = -\int_d^0 \tilde{C_D} D \sigma_u z dz \ \dot{\eta_1} - \int_d^0 \tilde{C_D} D \sigma_u z^2 dz \ \dot{\eta_5} = -B_{51}\dot{\eta_1} - B_{55}\dot{\eta_5} \tag{38}$$

For the conical part, the drag coefficient is the average of the values provided by [25] and $D = \frac{D_{OCtop} + D_{OCbot}}{2}$. The damping coefficients are identified in the same way, integrating the elementary forces over the length of the conical part.

For the circular ends of the pontoons, $D = D_{OCbot}$.

Central column

Only the central column's conical part is submerged. For this part, the drag coefficient is the average of the values provided by [25] and $D = \frac{D_{CCwl} + D_{CCbot}}{2}$, where D_{CCwl} is the diameter of the central column at the waterline.

Pontoon legs

The pontoons are subject to horizontal and vertical drag loads. The same drag coefficient is used for both. Let's write θ the angle between the global axis $\vec{x}$ and a leg axis $\vec{x'}$, and study a leg strip located at depth $h = -draft + \frac{H_{pont}}{2}$ and distance $x = x' cos(\theta)$ from the origin.
Then the normal component of that strip's horizontal velocity is $u_n = \left(\dot{\eta_1} + h\dot{\eta_5}\right)\sin(\theta)$. Let's write the drag force in the $\vec{x}$ direction and the corresponding moment $\vec{y}$:

$$dF_{D,1} = -\tilde{C_D} H_{pont} \sigma_{u_n} \left(\dot{\eta_1} + h\dot{\eta_5}\right)\sin(\theta)^2$$
$$dF_{D,5} = h dF_{D,1}$$

The corresponding damping coefficients are identified by integrating over the leg length, between $d_1 = a_{pont}$ and $d_2 = L_{pont} - b_{pont}$:

$$F_{D,1} = -\int_{d1}^{d2} \tilde{C_D} H_{pont} \sigma_{u_n} \sin(\theta)^2 dx' \ \dot{\eta_1} - \int_{d1}^{d2} \tilde{C_D} H_{pont} \sigma_{u_n} \sin(\theta)^2 h dx' \ \dot{\eta_5} = -B_{11}\dot{\eta_1} - B_{15}\dot{\eta_5}$$

$$F_{D,5} = -\int_{d1}^{d2} \tilde{C_D} H_{pont} \sigma_{u_n} \sin(\theta)^2 h dx' \ \dot{\eta_1} - \int_{d1}^{d2} \tilde{C_D} H_{pont} \sigma_{u_n} \sin(\theta)^2 h^2 dx' \ \dot{\eta_5} = -B_{51}\dot{\eta_1} - B_{55}\dot{\eta_5}$$

The vertical velocity of the leg strip is $w = -x' \cos(\theta)\dot{\eta_5}$. Let's now write the vertical drag force and the resulting pitch moment:

$$dF_{D,3} = \tilde{C_D} W_{pont} \sigma_w x' \cos(\theta)\dot{\eta_5}$$
$$dF_{D,5} = -x' \cos(\theta) dF_{D,3}$$

The corresponding damping coefficient is identified by integrating $dF_{D,5}$ over the leg length:

$$F_{D,5} = -\int_{d1}^{d2} \tilde{C_D} W_{pont} \sigma_w \left(x' \cos(\theta)\right)^2 dx' \ \dot{\eta_5} = -B_{55}\dot{\eta_5} \tag{39}$$

Heaveplates

The heaveplates are subject to only vertical drag forces. The bottom area is written A_{hp}. The vertical velocity of a heaveplate is $w = -L_{pont}\cos(\theta)\dot{\eta_5}$. Let's write the resulting moment on the heaveplate:

$$F_{D,3} = \tilde{C_D} A_{hp} \sigma_w L_{pont} \cos(\theta)\dot{\eta_5}$$
$$F_{D,5} = -L_{pont}\cos(\theta) F_{D,3} = -\tilde{C_D} A_{hp} \sigma_w \left(L_{pont}\cos(\theta)\right)^2 \ \dot{\eta_5} = -B_{55}\dot{\eta_5}$$

Member	C_D
OC top part	0.72
OC conical part	0.713
Circular edge	0.706
CC conical part	0.716
Pontoon leg	2.05
Heave plate	10

Table 1: Drag coefficient of the platform members

2.2.3 Hydrostatic restoring

The hydrostatic stiffness coming from the platform only is calculated as:

$$K_{\text{hydro},55} = \rho g I_{\text{wp}} + \rho g \nabla z_B - M_{\text{platform}} g z_{\text{g,platform}} \tag{40}$$

2.3 Aerodynamics

The aerodynamics on the turbine are highly simplified. The rotor and controller modeling is considered outside the scope and the power production is not of interest in the project. That is why the wind action on the nacelle is reduced to an excitation thrust force and a linear damping. The model uses thrust force spectra computed beforehand with the SIMA model of the DTU 10MW rotor. The spectra were generated using 1h simulations with a wind input using the Kaimal spectrum and the Kaimal exponential coherence model, with the normal turbulence model (NTM) for class B turbines [26]. The nacelle was considered fixed in space and the tower shadow effect for the baseline DTU10 MW tower was included.
Regarding the damping, a simple coefficient $B_{\text{aero}} = 1.25 \times 10^5$ kg/s is applied on the RNA.

2.4 Mooring

For each sea state, the mean thrust force from the wind yields a mean surge and pitch offset of the structure. The restoring forces from the mooring are linearized for each sea state around this mean position. The SIMA model with a finite element mooring description is used once again. Constant wind tests provide the offsets as a function of the wind speed. Then, at each mean position, a small pure force dF and a small pure moment dM are applied on the structure. The resulting small displacements $d\eta_1^{(dF)}$, $d\eta_5(dF)$, $d\eta_1^{(dM)}$ and

$d\eta_5(dM)$ are measured. Now if we write Q the inverse of the system's linear stiffness matrix, the following static equations can be written for each mean position:

$$\begin{bmatrix} d\eta_1^{(dF)} \\ d\eta_5^{(dF)} \end{bmatrix} = Q \begin{bmatrix} dF \\ 0 \end{bmatrix} \qquad \begin{bmatrix} d\eta_1^{(dM)} \\ d\eta_5^{(dM)} \end{bmatrix} = Q \begin{bmatrix} 0 \\ dM \end{bmatrix}$$

The coefficients of Q can then be obtained as:

$$Q_{11} = \frac{d\eta_1^{(dF)}}{dF} \qquad Q_{51} = \frac{d\eta_5^{(dF)}}{dF} \qquad Q_{15} = \frac{d\eta_1^{(dM)}}{dM} \qquad Q_{55} = \frac{d\eta_5^{(dM)}}{dM}$$

The sea state-dependent mooring stiffness matrix K_{moor} is obtained by inverting Q and removing the hydrostatic stiffness contribution from K_{55}. K_{moor} is considered constant throughout the optimization. It is worth noting that the main source of non-linearity in the mooring stiffness comes from the surge-surge coefficient. The pitch-pitch stiffness is close to being linear throughout the wind range.

2.5 Generalized displacements

The model uses generalized displacements to describe the response of the system as a weighted sum of arbitrary mode shapes $\psi(z) = [\psi_1(z) \;\; \psi_5(z) \;\; \psi_7(z)]$. The frequency dependent weights $x(\omega) = [x_1(\omega) \;\; x_5(\omega) \;\; x_7(\omega)]$ come from the equation of motion's solution. As mentioned before, three generalized degrees of freedom are considered, respectively surge, pitch and tower bending first mode. The surge and pitch mode shapes are known and are enforced as pure surge an pitch motion ($\psi_1(z) = 1$, $\psi_5(z) = z/h_{hub}$). However, the bending mode is unknown and may change significantly with the platform modification. It is therefore calculated by solving the eigenvalue problem of a simple finite element model. The FE model takes the platform and the RNA as lump masses and models the clamped tower with 2-dof beam elements. The hydrostatic and mooring restoring are modeled as point stiffness on the platform. The infinite frequency added mass coming from the potential flow solution is also taken into account. Once the eigenvalue problem is solved, a 4th order polynomial is fitted to the bending mode shape, in order to have analytical expressions for its first and second derivatives.

The generalized mass, damping and stiffness matrices are defined in equation 41, 42 and 43. The three modes are not orthogonal and will give rise to coupling effects, represented by off-diagonal elements in the generalized matrices. $\bar{K}$ has a contribution from the axial force in the tower $N(z)$, coming from the RNA and tower weight.

$$\begin{aligned} \bar{\mathbf{M}}(\omega) = &\int_{h_{\text{base}}}^{h_{\text{hub}}} m(z)\boldsymbol{\psi}(z)\boldsymbol{\psi}^\top(z)dz + M_{\text{platform}}\boldsymbol{\psi}(z_{\text{g,platform}})\boldsymbol{\psi}^\top(z_{\text{g,platform}}) + M_{\text{RNA}}\boldsymbol{\psi}(h_{\text{hub}})\boldsymbol{\psi}^\top(h_{\text{hub}}) \\ &+ I_{\text{platform}}\boldsymbol{\psi}_z(0)\boldsymbol{\psi}_z^\top(0) + A_{11}(\omega)\boldsymbol{\psi}(0)\boldsymbol{\psi}^\top(0) + A_{15}(\omega)\boldsymbol{\psi}(0)\boldsymbol{\psi}_z^\top(0) + A_{51}(\omega)\boldsymbol{\psi}_z(0)\boldsymbol{\psi}^\top(0) \\ &+ A_{55}(\omega)\boldsymbol{\psi}_z(0)\boldsymbol{\psi}_z^\top(0) \end{aligned} \tag{41}$$

$$\begin{aligned} \bar{\mathbf{B}}(\omega) = &B_{11}\boldsymbol{\psi}(0)\boldsymbol{\psi}^\top(0) + B_{15}\boldsymbol{\psi}(0)\boldsymbol{\psi}_z^\top(0) + B_{51}\boldsymbol{\psi}_z(0)\boldsymbol{\psi}^\top(0) + B_{55}\boldsymbol{\psi}_z(0)\boldsymbol{\psi}_z^\top(0) \\ &+ B_{\text{visc},11}\boldsymbol{\psi}(0)\boldsymbol{\psi}^\top(0) + B_{\text{visc},15}\boldsymbol{\psi}(0)\boldsymbol{\psi}_z^\top(0) + B_{\text{visc},51}\boldsymbol{\psi}_z(0)\boldsymbol{\psi}^\top(0) + B_{\text{visc},55}\boldsymbol{\psi}_z(0)\boldsymbol{\psi}_z^\top(0) \\ &+ B_{\text{aero}}\boldsymbol{\psi}(h_{\text{hub}})\boldsymbol{\psi}^\top(h_{\text{hub}}) \end{aligned} \tag{42}$$

$$\begin{aligned} \bar{\mathbf{K}} = &\int_{h_{\text{base}}}^{h_{\text{hub}}} EI(z)\boldsymbol{\psi}_{zz}(z)\boldsymbol{\psi}_{zz}^\top(z)dz + \int_{h_{\text{base}}}^{h_{\text{hub}}} N(z)\boldsymbol{\psi}_z(z)\boldsymbol{\psi}_z^\top(z)dz + K_{\text{hydro},55}\boldsymbol{\psi}_z(0)\boldsymbol{\psi}_z^\top(0) \\ &+ K_{\text{moor},11}\boldsymbol{\psi}(0)\boldsymbol{\psi}^\top(0) + K_{\text{moor},15}\boldsymbol{\psi}(0)\boldsymbol{\psi}_z^\top(0) + K_{\text{moor},51}\boldsymbol{\psi}_z(0)\boldsymbol{\psi}^\top(0) + K_{\text{moor},55}\boldsymbol{\psi}_z(0)\boldsymbol{\psi}_z^\top(0) \end{aligned} \tag{43}$$

The excitation loads considered in the model are the potential flow wave excitation forces on the hull and the thrust force on the rotor. The generalized force per unit wave height $\bar{\mathbf{F}}_w$ and the generalized force per unit wind load $\bar{\mathbf{F}}_U$ are given in equation 44 and 45.

$$\bar{\mathbf{F}}_{\mathrm{w}} = F_{\mathrm{exc},1}\boldsymbol{\psi}(0) + F_{\mathrm{exc},5}\boldsymbol{\psi}_z(0) \tag{44}$$

$$\bar{\mathbf{F}}_U = 1 \times \boldsymbol{\psi}(h_{\mathrm{hub}}) \tag{45}$$

2.6 Equation of motion

The dynamic equilibrium yields the following equation of motion in the generalized coordinates:

$$\bar{M}\ddot{x} + \bar{B}\dot{x} + \bar{K}x = \bar{F} \tag{46}$$

This equation is solved in the frequency domain. The conservative assumption of no interaction between the wave-induced and wind-induced response is made. It allows to superpose the wave-induced response spectrum and the wind-induced response spectrum to obtain the total response of the system. Assuming a periodic load of frequency ω, the linear system yields a periodic response $x = \tilde{x}e^{i\omega t}$ of the same frequency. For wave loads due to regular waves with unit amplitude, the equation of motion becomes:

$$\left[-\omega^2\bar{M} + i\omega\bar{B} + \bar{K}\right]\tilde{x}e^{i\omega t} = \bar{F}_{\mathrm{w}}e^{i\omega t}$$

A complex transfer function for the responses due to a unit wave amplitude can be established as in 47. It contains information about the amplitude and the phase of the response.

$$H_{x,\mathrm{w}}(\omega) = \left[-\omega^2\bar{M} + i\omega\bar{B} + \bar{K}\right]^{-1}\bar{F}_{\mathrm{w}} \tag{47}$$

The response for each degree of freedom to a wave spectrum S_{w} is calculated as:

$$S_{x_k,\mathrm{w}} = |H_{x_k,\mathrm{w}}|^2 S_{\mathrm{w}} \tag{48}$$

Similarly, a transfer function for the response due to unit thrust force can be established:

$$H_{x,U}(\omega) = \left[-\omega^2\bar{M} + i\omega\bar{B} + \bar{K}\right]^{-1}\bar{F}_U \tag{49}$$

And the response for each degree of freedom to a thrust force spectrum S_{F_U} is calculated as:

$$S_{x_k,U} = |H_{x_k,U}|^2 S_{\mathrm{F}_U} \tag{50}$$

To find the total response of the system, the contribution from the waves and the wind are added together:

$$S_{x_k} = S_{x_k,U} + S_{x_k,\mathrm{w}} \tag{51}$$

To compute the viscous damping, the transfer functions of the response derivative are needed. They are calculated as:

$$H_{\dot{x},\mathrm{w}}(\omega) = i\omega H_{x,\mathrm{w}}(\omega) \qquad H_{\dot{x},U}(\omega) = i\omega H_{x,U}(\omega)$$

For a given spectrum S, the spectral moments are calculated as:

$$m_k = \int_0^\infty \omega^k S(\omega)\mathrm{d}\omega$$

The standard deviation is then defined as $\sigma = \sqrt{m_0}$.

2.7 Environmental conditions

The environmental conditions that are considered are both operational load cases and extreme load cases. The wave conditions are modeled through Jonswap spectra with a peak parameter $\gamma = 3.3$. The wind conditions are modeled through thrust force spectra. The design basis from Life50+ [27] provides the normal sea states for the fatigue study (table 2) and the extreme sea state with a return period of 50 years for the ultimate strength analysis (table 3). The turbine is parked for the extreme sea state.

U_{hub} [m/s]	H_s [m]	T_p [s]	P [%]
4	1.38	5	3.45
6	1.38	7	6.89
4	1.38	11	3.45
6	1.67	5	5.99
8	1.67	8	11.98
6	1.67	11	5.99
10	2.2	5	6.41
10	2.2	8	12.83
10	2.2	11	6.41
14	3.04	7	5.12
14	3.04	9.5	10.24
14	3.04	12	5.12
18	4.29	7.5	2.9
18	4.29	10	5.81
18	4.29	13	2.9
20	6.2	10	0.94
20	6.2	12.5	1.88
20	6.2	15	0.94
20	8.31	10	0.19
20	8.31	12	0.37
20	8.31	14	0.19

Table 2: Operational environmental conditions for fatigue study

U_{hub} [m/s]	H_s [m]	T_p [s]
44	10.9	16

Table 3: Extreme environmental conditions with a 50-year return period

3 Optimization problem

This section gives the framework of the optimization problem, its objective function, design variables and constraints. To keep the project to a reasonable extent, the optimization only focuses on the semi-submersible geometry. The mooring system, the tower, the turbine and internal structure of the system are not modified and the optimization is narrowed down to a simpler and single-disciplinary problem.

3.1 Objective function

Solving an optimization problem of this kind eventually goes down to finding the "best design possible". In the case of a FWT, the best design can be seen as the one producing the most energy at the cheapest cost (for a constant lifetime). This is once again equivalent to minimizing the LCOE of the system. The deliverable D2.2 of the Life50+ project [28] details the calculation of a floating wind turbine LCOE. Just like any power production facility, the LCOE for a set lifetime is defined as

$$\text{LCOE} = \frac{\text{Life cycle cost}}{\text{Electrical energy provided}}$$

The first factor here, the amount of energy produced throughout the FWT's life, depends mostly on its geographical location and the efficiency of the turbine control system. Since these parameters are fixed in this study, the optimization will not influence the power production. The second term, the life cycle cost, typically includes CAPEX for capital expenses, OPEX for operation and maintenance expenses and decommissioning expenses DECEX. OPEX and DECEX will not be affected in this study and are removed from the scope. Going further down the CAPEX, only the manufacturing cost of the floating substructure is of interest here. The mooring system characteristics are kept constant and the potential changes in its dimensions due to changes in the floating substructure size will have a negligible impact on the cost. In the same way, the turbine and the tower are kept constant during the optimization. The cost C_{FS} of a the floating substructure can be written as the sum of three factors:

$$C_{FS} = TC_{LC} + TC_{MC} + TC_{OC}$$

Where TC_{LC} is the total labor cost, TC_{MC} is the total manufacturing cost and TC_{OC} is the total overhead cost. If the floating platform has n components to be manufactured with p different materials, then

$$TC_{LC} = \sum_{i=1}^{n} t_{FSi} \times c_{LCi}$$

$$TC_{MC} = \sum_{i=1}^{n} \sum_{j=1}^{p} m_{ij} \times c_{ij}$$

where t_{FS} is the manufacturing time, c_{LC} the hourly labor cost, m is the mass of the material and c is the cost of the material. Overhead costs are directly related to the manufacturing process and one way to account for them is to apply a percentage of the manufacturing cost. Given that the general geometry of the floater is already defined and that the optimization will only change the length of some components, it can be assumed that these costs won't be affected by the optimization and they are hence not taken into account.

The price of concrete being negligible in front of the price of steel, a simple cost model of the platform is its mass of steel. The objective function to minimize is chosen to be M_{steel}.

3.2 Design variables

The design variables are only geometrical and are chosen among the dimensions listed in 6. To keep the geometry changes simple, especially for the meshing automation, L_{pont} and D_{OC} are taken as design variables. This means that all the other parameters that are independent of L_{pont} and D_{OC} are kept constant.

3.3 Constraints

The more constraints are established, the larger the computational effort will be. Therefore, the challenge is to limit their number by understanding which constraint is already included in which constraint. For example, it might not be necessary to restrict the motions of the system if the stresses in different components are already checked. In this section, the optimization constraints are determined in that philosophy.

The definition of the constraints is based to a large extent on the requirements presented in the DNVGL standards [29]. Following common design practices, the structure must be checked according to ultimate limit state (ULS) and fatigue limit state (FLS). Basic requirements are also imposed to keep the design realistic. The constraints on maximum values apply to every considered sea state and use a 3h duration.

3.3.1 Constraints related to the platform

Since no structural model of the platform is used, the constraints on the semi-submersible will be related to only its rigid body response. First and very basic, the platform must float with the correct draft. Ballast will be adjusted to balance the buoyancy with the weight of the whole system. The ballast mass is therefore required to be positive.
A maximum surge displacement of 30 m is defined to avoid rupture of the power cables. This value is chosen based on the original system's response to environments characterized by a wind speed close to rated: for typical operational sea states with $U = 10$ m/s, the maximum surge excursion is 28m. No modeling of the tension in the mooring lines was done and so no constraint on a maximum tension can be applied. The limit on the surge motion will therefore also serve as a mooring constraint.
A stability check based on the calculation of the area below the stability curve is usually required. To avoid such calculation, it is typically assumed that setting a limit for the static pitch angle under rated wind speed is enough to ensure sufficient static intact stability. A limit of 5 deg is therefore defined for the static pitch angle. [27] also requires a maximum dynamic pitch angle of 10 deg in operational conditions.
Finally, since the model doesn't include the heave degree of freedom, a constraint on the natural heave period is necessary to control that motion. T_3 can not be smaller than 20s, to avoid being in the wave frequency range.

3.3.2 Constraints related to the tower

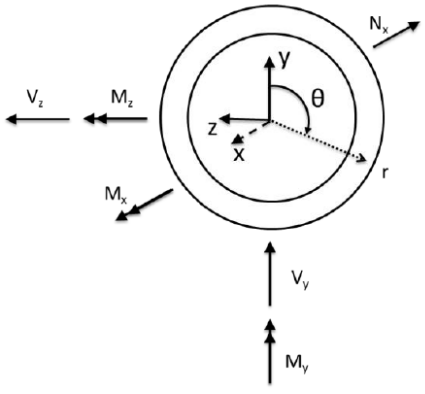

Figure 9: coordinate system for the structural analysis of a tower section

The stresses inside the tower arise from the axial force N_x and bending moment M_y. N_x comes from the weight of the RNA and the tower, and is constant through time and optimization. M_y is calculated using the curvature of the bending mode shape. Normally, the stresses around the whole circumference of the tower should be checked, but with a 2D model subject to aligned wind and waves, only the point $\theta = 90°$ on the outer radius can be checked. The resulting axial stresses at that point are calculated as:

$$\sigma_x(z,\omega) = \frac{N_x(z)}{A(z)} - \frac{M_y(z,\omega)}{I_y(z)} r = \frac{N_x(z)}{A(z)} - EI_y(z)\psi_{zz}(z)\tilde{x}_7(\omega)\frac{r(z)}{I_y(z)}$$

A linear relation can be established between the generalized bending response $\tilde{x}_7$ and the bending stress:

$$H_{\sigma_M}(z) = -E\psi_{zz}(z)r(z)$$

The response spectrum of the bending stress along the tower is then:

$$S_{\sigma_M}(z,\omega) = |H_{\sigma_M}(z)|^2 S_{x_7}(\omega) \tag{52}$$

The fatigue analysis of the tower is performed with the SN curve methodology, under the assumption of linear cumulative damage. The SN curve gives the number of cycles to failure given a stress range. The analysis is here based on the SN curve D from table 2.1 in [30] (figure 10). S-N curves are different for axial stress and shear stress. Here we focus only on the axial stress since it's usually the most critical. Since the SN curve method relies on stress ranges, only the dynamic stresses (due to M_y) are of interest in the fatigue study.
To compute the fatigue damage for a specific sea state, we apply the Dirlik's method [31]. It is a stochastic method using the spectral moments of the bending stress response spectrum. The fatigue damage during T seconds according to Dirlik is:

$$D_{\mathrm{DK}} = \frac{v_p T}{K}(2\sigma)^m \left(G_1 Q^m \Gamma(1+m) + (\sqrt{2})^m \left(G_2 R^m + G_3\right)\Gamma\left(1+\frac{m}{2}\right)\right)\left(\frac{t}{t_{\mathrm{ref}}}\right)^{mk} \tag{53}$$

Where

$$G_1 = \frac{2\left(x_m - \alpha_2^2\right)}{1+\alpha_2^2}\ ,\ G_2 = \frac{1-\alpha_2-G_1+G_1^2}{1-R}\ ,\ G_3 = 1-G_1-G_2\ ,\ Q = \frac{1.25\left(\alpha_2 - G_3 - G_2 R\right)}{G_1}\ ,\ R = \frac{\alpha_2 - x_m - G_1^2}{1-\alpha_2-G_1+G_1^2}$$

and

$$\alpha_2 = \frac{m_2}{\sqrt{m_0 m_4}}\ ,\ x_m = \frac{m_1}{m_0}\sqrt{\frac{m_2}{m_4}}\ ,\ v_p = \frac{1}{2\pi}\sqrt{\frac{m_4}{m_2}}$$

In equation 53, m and $K = \bar{a}$ are the parameters of the first part of the SN curve, where $N \leq 10^7$ cycles. By summing the fatigue damage of all the considered sea states, weighted by probabilities of occurrence, the design criterion is given in equation . The FWT is designed for a 25-year lifetime. According to [29], the design fatigue factor is taken equal to DFF = 1.

$$\mathrm{DFF}.D_{25y} \leq 1 \tag{54}$$

The ultimate strength capacity of the tower in yielding must be assessed. Since the system was made linear, a Gaussian wave process will yield a Gaussian bending stress response. Therefore, the maxima distribution in a S_{σ_M} realization will follow a Rayleigh distribution, and the expected largest bending stress during a sea state of 3h is given by:

$$\sigma_{\max,3\mathrm{h}} = \sigma_\sigma\left(\sqrt{2\ln N_{3\mathrm{h}}} + \frac{0.5772}{\sqrt{2\ln N_{3\mathrm{h}}}}\right) \tag{55}$$

Where $N_{3\mathrm{h}}$ is the number of individual maxima in 3h and σ_σ is the standard deviation of S_{σ_M}. The tower is considered safe if the axial stresses never exceed the steel yield stress all along the tower:

$$\gamma_f\left(\sigma_{\max,3\mathrm{h}} + \frac{N_x}{A}\right) \leq \frac{\sigma_y}{\gamma_m}$$

Here, the partial safety factor for the material is $\gamma_m = 1.1$ according to [32]. The partial safety factor for the load is $\gamma_f = 1.35$ according to [29].

No constraint on buckling of the tower was applied. Axial stresses are typically studied for the buckling assessment, and here the dead weight of the turbine is the main contributor. Since the tower design will not change during the optimization, we just have to check that the initial design is safe regarding buckling.

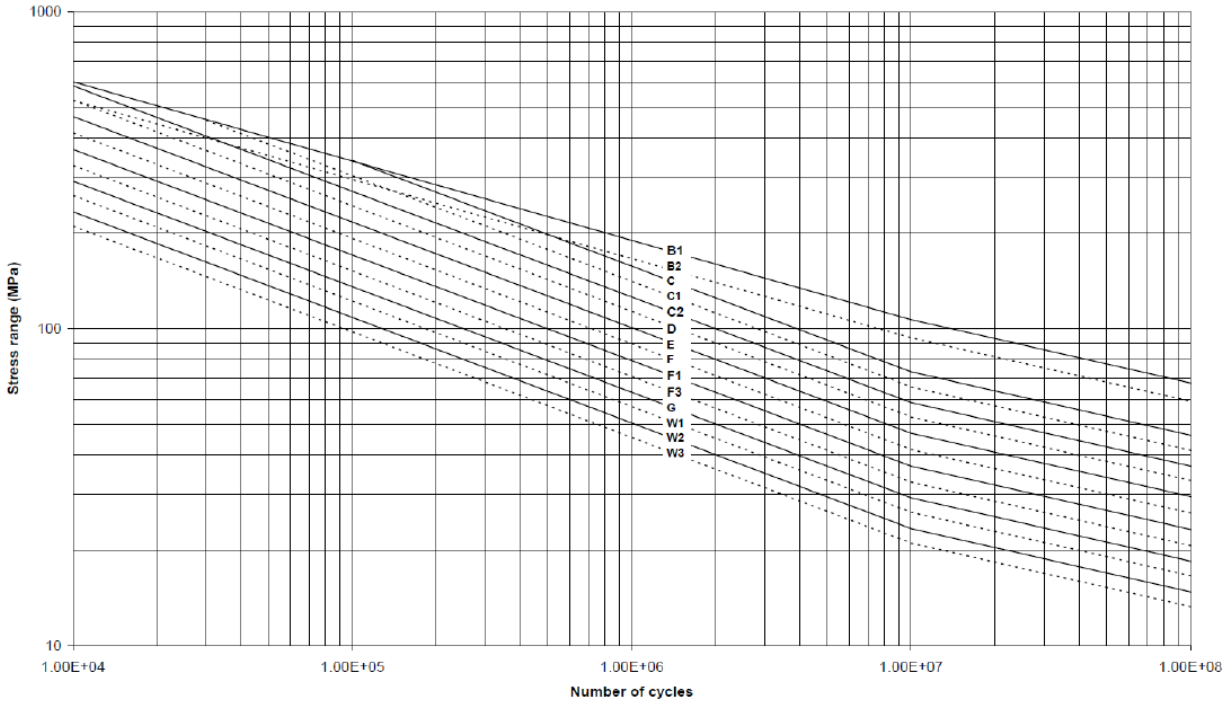

Figure 10: SN curve in air

Property	Value	Unit
Young's modulus E	210	GPa
Poisson's ratio ν	0.3	-
Mass density ρ	7855(8500)	kg/m^3
Minimum yield strength σ_y	355	MPa

Table 4: Properties of the tower steel

3.4 Calculation of derivatives

Since the panel meshing and potential solver are black boxes and we don't have access to the code, the only solution to approximate the derivatives of the hydrodynamic coefficients is to use finite differences. This dramatically increases the run time since the potential solver must be run another time to compute the partials. For the rest of the model, time constraints didn't allow to provide analytical partials to every components. Analytical partial derivatives are calculated for all the components related to the platform geometry, the mass model and the viscous forces. All the remaining components are attributed finite-difference partials.

4 Training model

A first optimization process was carried out with a very basic model to get the hang of such a procedure. This model doesn't relate in any way to the studied OOStar, but the model structure is similar. The idea is to practice and get used to working in the OpenMDAO environment with a model that can be visualized and verified easily. Once the concepts of objective function, constraints, and convergence were handled correctly, the more advanced model was be developed.

This "training model" is a catenary-moored floating cylinder, similar to a spar, supporting a dead weight corresponding to the 10MW DTU wind turbine. The problem is solved in the frequency domain and the model simply looks at the linear rigid body response of the floater in the (x, z) plane for one given sea state. Only the surge and pitch degree of freedom are included. Only wave excitation is considered, no wind input. The spar is described by its diameter D, draft d, freeboard fb and a constant wall thickness of $t_w = 10$ cm.

The model relates very little to reality and the results are to be taken purely illustratively. Once again the purpose is to be able to assess a correct optimized result.

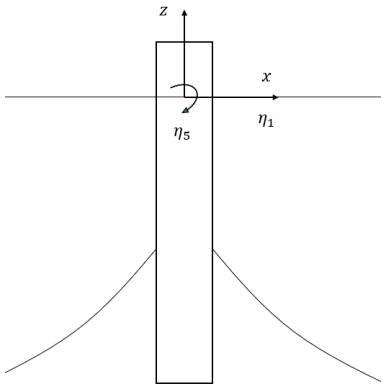

Figure 11: Sketch of the training model

4.1 Description of the training model

The training model follows the same logic as the real model, but in a very simplified version. Just like the real model, the training model solves the following equation of motion:

$$(M + A)\,\ddot{\eta} + B\dot{\eta} + K\eta = F_{\text{exc}}$$

The mass matrix is calculated in the following way: D and d yield the submerged volume and the displacement of the system, 23% of which is allowed to the steel mass, eventually ballasts are filled up from the bottom so that $M_{\text{steel}} + M_{\text{DTU10MW}} + M_{\text{ballast}}$ equals the displacement. The added mass matrix is approximated using the the analytical expression for a 2D circular cylinder with diameter D in infinite fluid [34]:

$$a_{11} = \rho\pi D^2/4$$

The damping of the system is modeled here as purely viscous and formulated again by a stochastic linearization of the Morison drag term [24]. The elementary transverse force on a cylinder strip with $C_D = 0.7$ is:

$$dF_{D1} = -\frac{1}{2}\rho C_D D\,(\dot{\eta_1} + z\dot{\eta_5})\,|\dot{\eta_1} + z\dot{\eta_5}| \approx -\frac{1}{2}\rho C_D D\sqrt{\frac{\pi}{8}}\sigma_{\dot{\eta_1}+z\dot{\eta_5}}\,(\dot{\eta_1} + z\dot{\eta_5})$$

The linear wave excitation forces are approximated using the diffraction forces from MaxCamy-Fuchs theory [35]. The horizontal force per unit length on the cylinder strip due to a regular wave of unit amplitude is given by:

$$dF_{exc} = \frac{4\rho g}{k} \frac{\cosh k(z+h)}{\cosh(kh)} G e^{i(\omega t - \alpha)}$$

$$\frac{1}{G} = \sqrt{J_1'(k\frac{D}{2})^2 + Y_1'(k\frac{D}{2})^2} \quad \text{and} \quad \tan(\alpha) = \frac{J_1'(k\frac{D}{2})}{Y_1'(k\frac{D}{2})}$$

The stiffness matrix is composed of the hydrostatic restoring and the mooring restoring, linearized around 0 thanks to the SIMA model.

4.2 Definition of the training optimization

The optimization of the training model is similar to the complete one but simplified. The objective function to minimize is the mass of steel. The two design variables are the diameter D and the draft d of the platform. The first constraint is about static equilibrium, the ballast mass needs to be positive so that the cylinder floats. Basic stability requires that the pitch restoring stiffness is positive. Furthermore, the static pitch angle under rated thrust is typically limited to 5 degrees. Finally, to limit the motions of the floater, an upper limit on the surge and pitch response standard deviation is imposed. These limits are not based on any standard, they are arbitrary values, chosen simply to build the optimization.

To sum up, the training optimization problem can be written as follows:

$$\begin{array}{rl} \text{minimize} & M_{steel} \\ \text{with respect to} & D \in [2\text{ m}, 25\text{ m}] \quad \text{and} \quad d \in [50\text{ m}, 150\text{ m}] \\ \text{subject to} & M_{ballast} > 0 \\ & K_{55} > 0 \\ & \eta_5 < 5° \quad \text{for } F_{thrust} = 1.5\text{e}6\ N \\ & \sigma_{\eta_1} < 5\text{m} \\ & \sigma_{\eta_5} < 0.075° \end{array}$$

For simplicity, only one sea state is used in this problem. It is characterized by a Jonswap spectrum with the parameters $H_s = 6.2$m, $T_p = 12.5$s and $\gamma = 3.3$. The SciPy SLSQP optimizer is used and all the derivatives are computed with finite difference.

4.3 Visualization of the training problem

The main advantage of this model is the possibility to plot the values of interest. By evaluating the objective function and the constraints throughout the design space defined by D and $draft$, the surfaces and contours in figure 12 can be obtained.

The objective function here is very simple and increases logically with the diameter and the draft. The ballast mass increases in the same direction. The constraint on the standard deviation of the surge and pitch response prevents the structure to have (1) a too large diameter, which would result in large wave loads, and (2) a too small draft which would reduce the stability of the platform. Finally, the instability showed by the rated pitch constraint going to infinity occurs when the pitch stiffness goes to zero: at some point, the CoG goes above the CoB and $\rho g V Z_B - M g Z_G$ becomes negative. When it exceeds the waterplane area stiffness contribution, K_{55} becomes negative and the platform is unstable. Therefore, we have to remember that the part of the design space outside this pitch angle "barrier" is not physical because the platform is not stable.

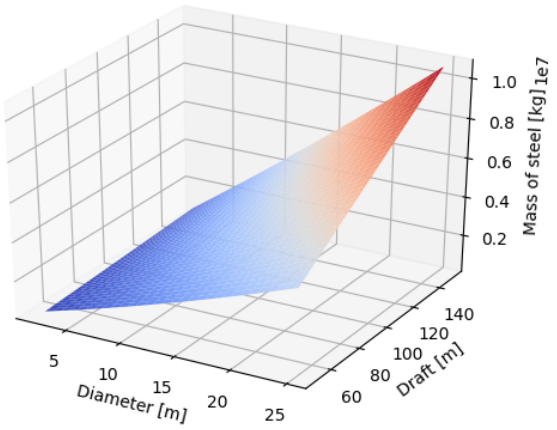

(a) Objective function: mass of steel

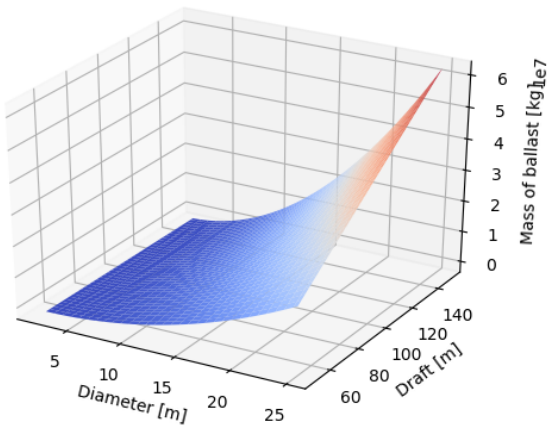

(b) Mass of ballast - must be > 0

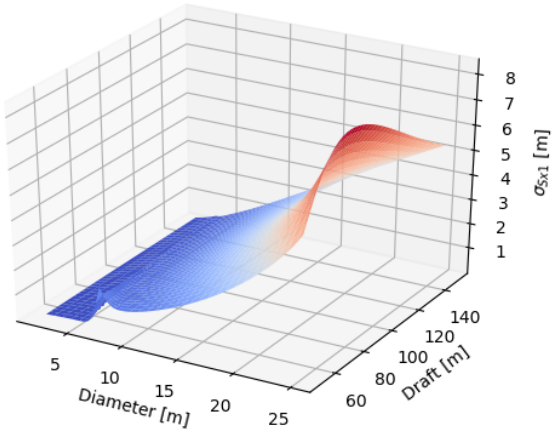

(c) Standard deviation of the surge response for the studied sea state - must be < 5m

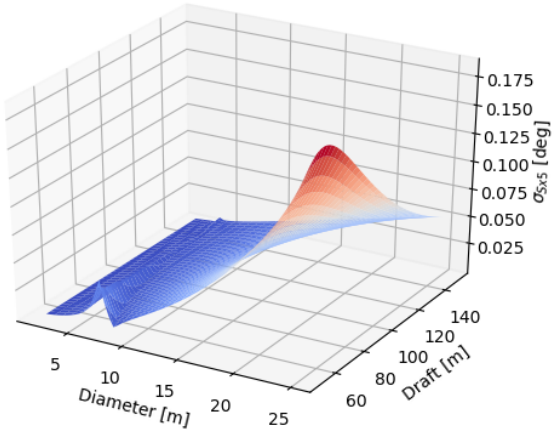

(d) Standard deviation of the pitch response for the studied sea state - must be < 0.075deg

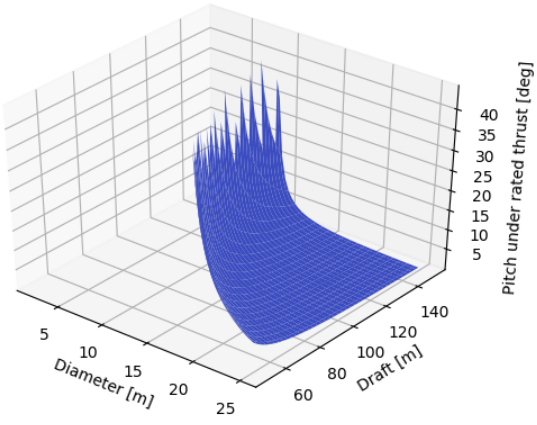

(e) Static pitch angle under rated thrust - must be < 5deg

Figure 12: Surface plots of the objective function and the constraints of the training model

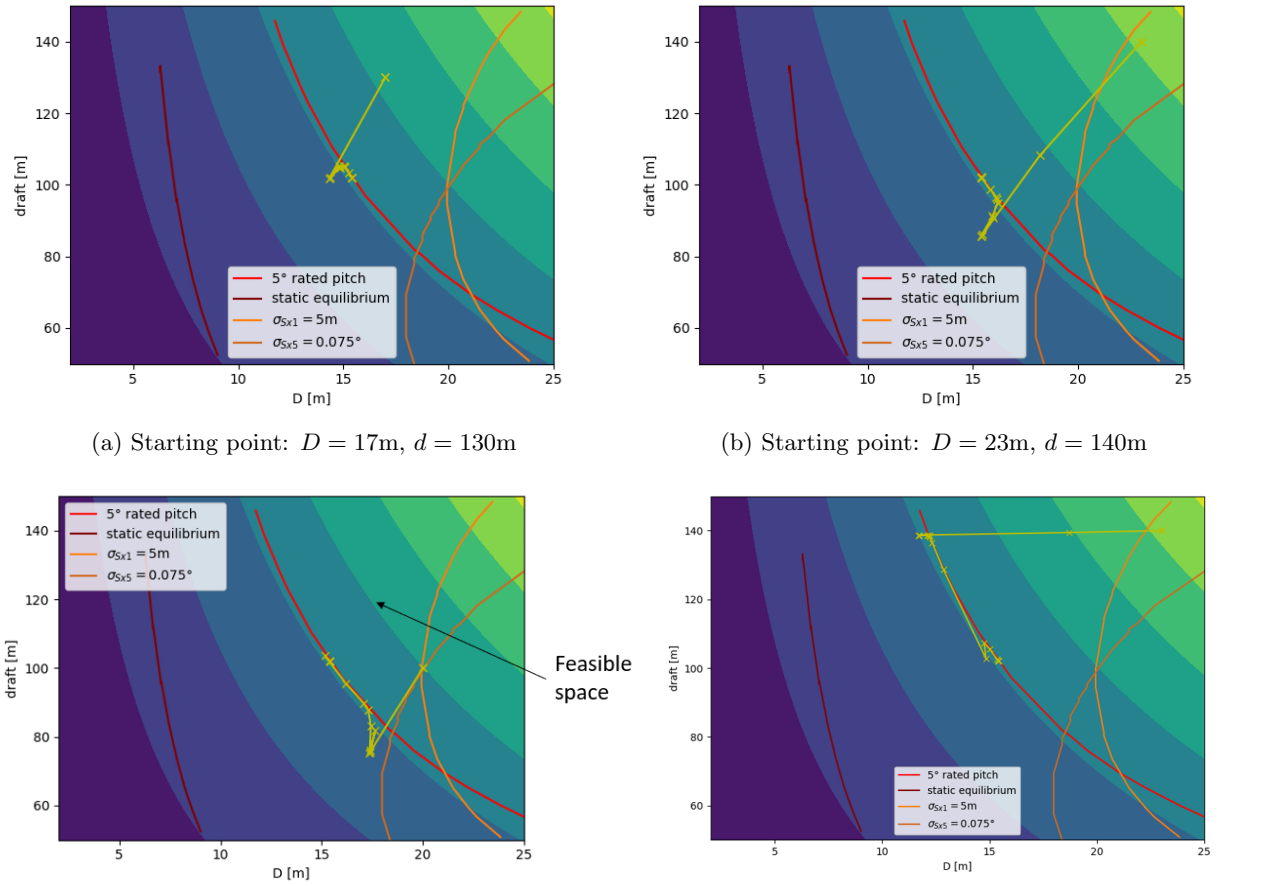

(a) Starting point: $D = 17$m, $d = 130$m

(b) Starting point: $D = 23$m, $d = 140$m

(c) Starting point: $D = 20$m, $d = 100$m

(d) Starting point: $D = 23$m, $d = 140$m, draft not scaled

Figure 13: Iterations of the optimization in the design space, with objective function and constraints represented

4.4 Results and observations of the training optimization

The optimization was carried out for three different starting points, to check the behavior of the optimizer in different conditions. The results are shown graphically in figure 13 and the details are given in table 5. On the graphs, the background is the contours of the objective function, the curves represent where the constraints are equal to their limit value, and the yellow dots describe the optimization path. The feasible space is therefore located above the rated pitch constraint and on the left of the standard deviation constraints. The actual values of the solutions are not of interest since the training model is not meant to represent a real platform. However the way the optimizer finds that solution, as well as potential errors, can teach multiple lessons about how the optimization works.

The first observation is that the constraint on the static pitch angle under rated thrust is a clear "wall" to minimizing the mass of steel. The optimized solution is therefore expected to be on that red line, where the pitch angle is the maximum tolerated. In other words, the rated pitch constraint will be active at the solution and would represent a driving constraint for the platform design. A consequence is that the constraint on the ballast mass to be positive to make the platform float is useless. It could never be active because of the rated pitch constraint. With a bit of thinking, it could have been anticipated that a static stability requirement would prevent the floater from becoming so small that it would not float anymore. Removing a constraint would save some computational time.

Another observation is that the optimizer first uses a direction close to the steepest descent, without apparently accounting for constraints. Once it crosses the pitch constraint, it goes back and then follows the constraint until reaching the solution. A consequence is that the algorithm allows unfeasible points. It doesn't seem to be a problem here but we need to remember that the model should be robust enough to support dealing with potentially non-physical designs. The results also shows that starting from an unfeasible point ($D = 23$m and $d = 140$m) can be acceptable.
This specific optimization problem proved to be quite tricky because the driving pitch constraint is almost parallel to the steel mass contour. Therefore knowing that the solution would be on the constraint is not enough to guess where the optimum is. This shows how useful and efficient optimization algorithm are.
An important lesson from this exercise is how sensitive the optimization is to scaling. To get the results in figure 13, the objective function, the design variables and the constraints were scaled so that their value stay in the same range of magnitude. The subfigure d in figure 13 shows an example of a run where only the draft was not scaled. One can see that the difference in magnitude between the two design variables causes the optimizer to prefer a horizontal, and therefore less direct, path. A badly scaled problem could even cause the optimizer not to converge if, e.g. a constraint is too dominating.

	Opti 1	Opti 2	Opti 3
Starting point	[17,130]	[20,100]	[23,140]
Iterations	12	14	17
Function evaluations	12	14	19
Gradient evaluations	12	14	17
Optimum	45.93742322	45.93742348	45.93742349
Location of the optimum	[15.40920667 , 102.10189288]	[15.40921865 , 102.10179362]	[15.40921942 , 102.10178723]
Rated pitch at optimum	5	5	5
σ_{η_1} and σ_{η_5} at optimum	[3.18355074 , 0.04499912]	[3.1835544 , 0.04499922]	[3.18355463 , 0.04499923]

Table 5: Results of the training optimization

5 Results and application of the model

In order to assess the validity of the model, the first part of this section presents a comparison between the system's performances predicted by the linear model and the state-of-the-art non-linear SIMA model. The linear model and the optimization set up are complete. Unfortunately, time was missing to carry out the whole optimization. However, the purpose of the project was also to build an efficient model that could provide a quick insight into the consequences of modifying the design. That's why the second part of this section investigates 9 different points of the design space, trying to determine manually some design-driving patterns.

5.1 Validation of the model

This part looks at the results given by the linear model and the SIMA model for the original design. Comparing the two is a way to check if the linear results are consistent. It must be recalled here that the linear model represents a steel platform, instead of concrete. Therefore the mass distribution is not the same. Essentially, the center of mass of the platform is 2m lower in the linear model than the original reference platform, and the pitch moment of the platform is greater. Added to the simplifications inherent to the model, it must be said that the point of the validation is not to match the SIMA results perfectly. It is rather to make sure the linear model captures the essential dynamics of the FWT.

Figure 16 shows the first bending mode shape of the original design calculated with the FEM component within the linear model. The shape makes sense and its natural frequency $\omega_7 = 4.4$ rad/s is close to the reference (4.9 rad/s). The fitted polynomial is used to calculate ψ_z and ψ_{zz}.

Figure 14 shows the standard deviation of the surge, pitch and bending moment response to the operational sea states. The linear results follow quite well the trend of the integrated model before rated wind speed. However, the surge motions are overestimated for most wind speeds. A reason for that can be the mooring modeling. Since the mooring restoring is the only source of stiffness in the surge motion, the approximations resulting from its linearization is likely to cause the overestimation. The pitch motions are largely underestimated for above-rated wind speeds. A reason for that can be the aerodynamics modeling. A constant damping coefficient was simply applied on the RNA, while the real aerodynamic damping forces depend to a large extent on the rotor state, e.g. blade ptich, and the wind speed. The bending moment looks closely coupled with the pitch motion and present the same gaps with the SIMA results.

More information about these differences can be found by looking at the response spectra in figure 15. The first thing to notice is that the linear model has a good estimation of the natural frequencies, around 0.038 rad/s in surge and around 0.22 rad/s in pitch. The natural frequency of the first tower bending mode lies away from any excitation, not contributing to the response and therefore not shown on the graphs. The spectra show that the system's response to waves is correctly assessed by the linear model. The energy is located in the same frequency range for the linear and the SIMA model. On the contrary, the response at lower frequencies, triggered by wind forces, are quite different between the two models and explain the discrepancies visualized in the standard deviations. The linear response at the surge frequency is too large compared to the response at the wave frequencies. The linear response at the pitch frequency is too small and too much energy is attributed to frequencies close to 0 rad/s. This shows the limit of modeling the rotor interaction with the wind simply with a thrust force and constant damping.

Figure 17 shows the 25-year fatigue damage along the tower. Confirming what previous studies on the 00Star showed, the fatigue critical point is not at the tower base but further up. With the SIMA model giving a 25y fatigue damage of 0.224 at the tower base, it appears however that the fatigue damage estimated by the linear model is largely underestimated. A reason for that is the mentioned inaccuracy in the system's response to wind. In a smaller extent, the Dirlik fatigue calculation method also brings limitations because it uses only one part of the S-N curve.

To sum up, the linear model captures pretty well the hydrodynamics of the system and therefore its response to waves. On the other side, the aerodynamics modeling seems to be unsatisfactory to represent the response to wind. In a general way, the trends in motion and bending moment response are correctly represented for below-rated wind speeds, where wave action dominates but get away from reality for above-rated wind

speeds, where wind action takes over. The fatigue calculation along the tower yields the correct vertical distribution, with the maximum damage occurring at around 43% of the tower length. The underestimation in absolute value makes it delicate to implement a fatigue constraint in the optimization, but it can at least be used in a relative way to compare different designs. The linear model doesn't match the OOStar results but captures well enough the FWT dynamic trends to compare different designs of steel platforms.

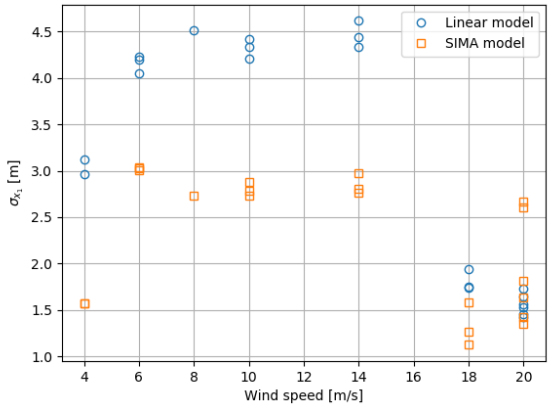

(a) Standard deviation of the surge response

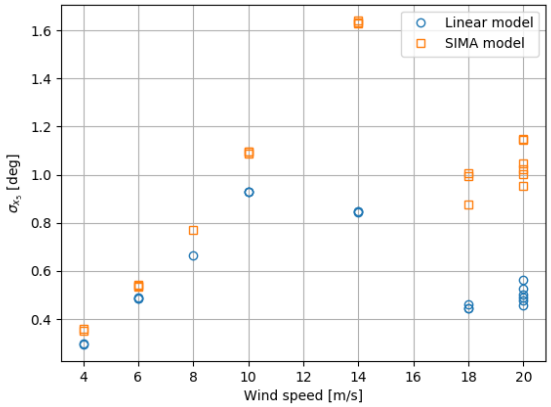

(b) Standard deviation of the pitch response

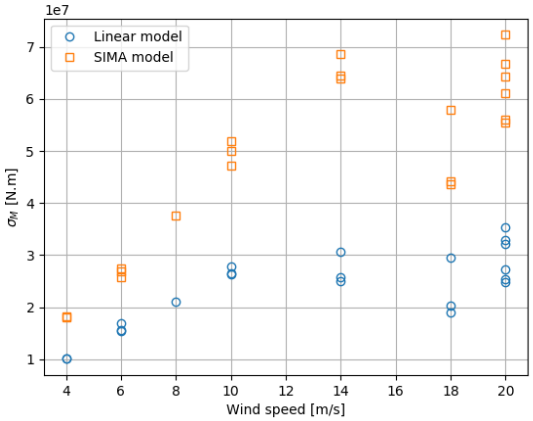

(c) Standard deviation of the tower base bending moment response

Figure 14: Standard deviation of the original design's response to operational sea states

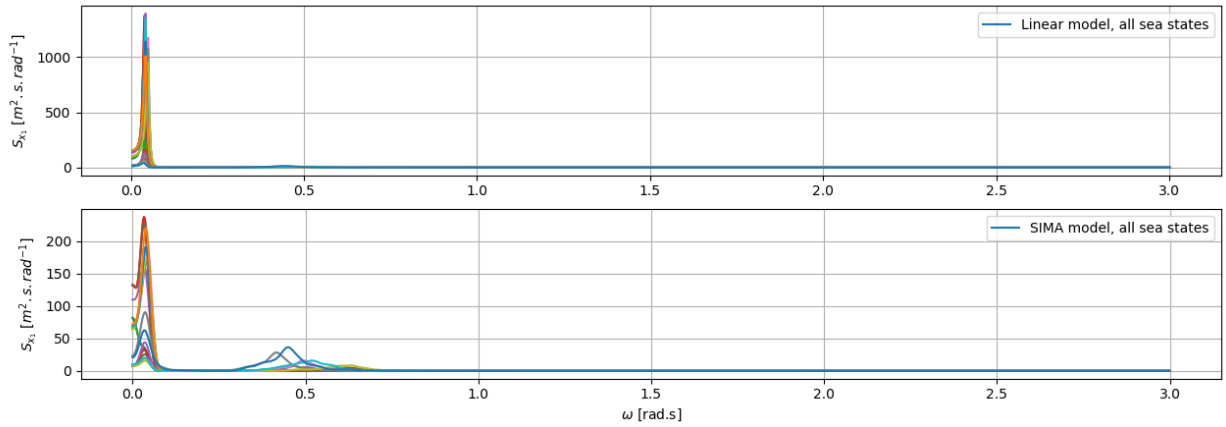

(a) Surge response to every operational sea states

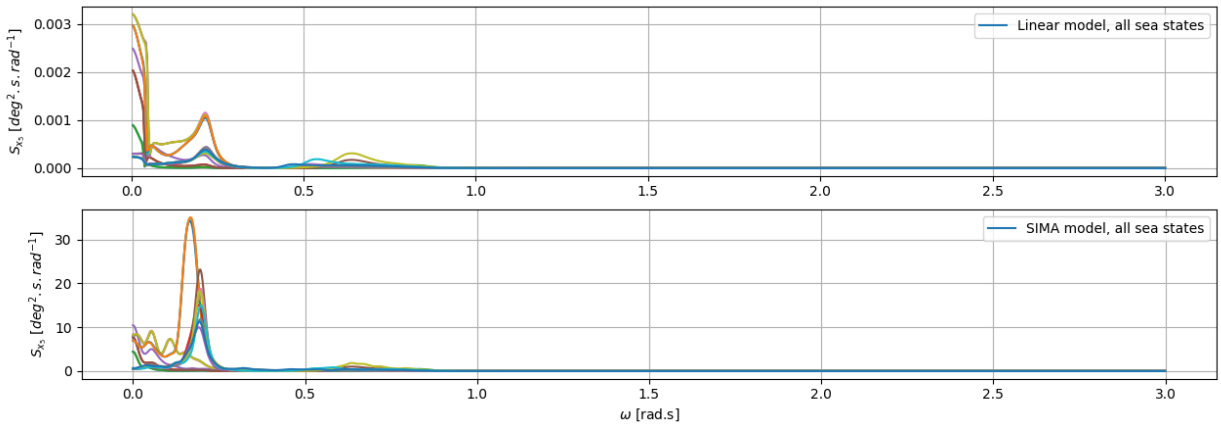

(b) Pitch response to every operational sea states

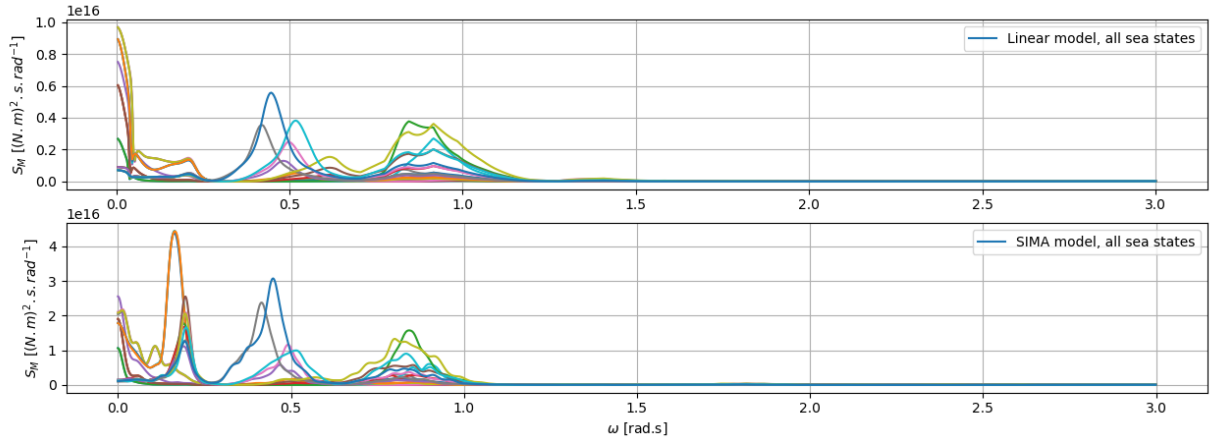

(c) Tower base bending moment response to every operational sea states

Figure 15: Comparison between the response of the original design predicted by the linear model and the SIMA model

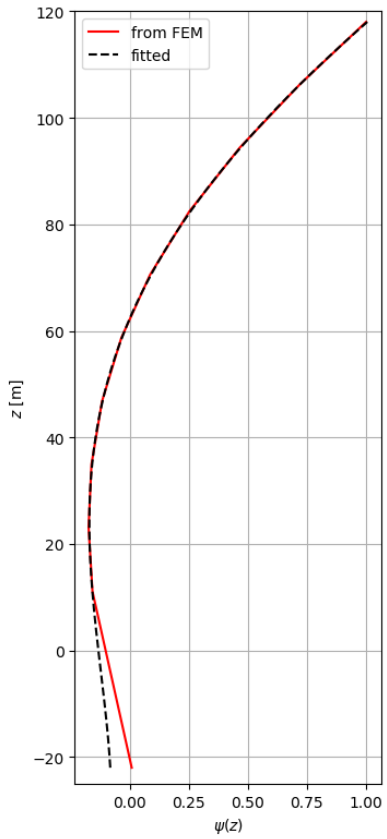

Figure 16: First bending mode shape of the original design - $\omega_7 = 4.4$ rad/s

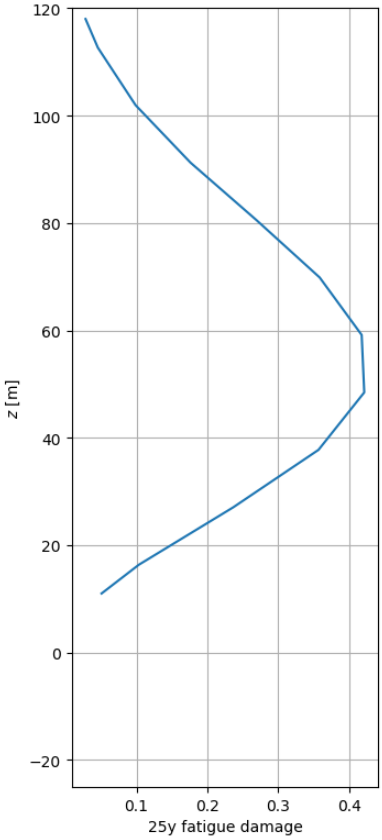

Figure 17: 25-year fatigue damage from tower base to tower top of the original design

5.2 Exploration of the design space

Time was missing to perform the full optimization on the linear model. But since every calculation in the model was automated for that purpose, it is very easy to change the values of the design variables L_{pont} and D_{OCtop} and look at the consequences in the system's performances. This part makes use of that model strength to explore the design space manually and investigate 9 new designs.

Table 6 makes a summary of the linear model results for D0 the original model and D1-9 the new designs. It includes the value of the design variables, the objective function M_{steel}, the degree of freedom natural frequencies and some of the optimization constraints: maximum displacement in surge and pitch, maximum bending moment at the tower base and heave natural frequency. Figures 18 and 19 superpose the standard deviations and 25y fatigue damage of every D_i.

D2, D6 and D9 present a negative generalized pitch stiffness, due to a too small hydrostatic restoring. These designs are therefore not stable. Looking at the other designs in the graphs, it is clear that changing the design variables doesn't change the trend of the responses. The standard deviations and the fatigue results have the same shape for every design but they change in magnitude. Keeping the overall shape of the platform (3-legged semisub with columns) fixed, the overall behavior of the system is also fixed. None of the designs give rise to a new trend in surge, pitch, bending moment or fatigue response.

The table gives more insight into the trade-offs. All the designs reduce the mass of steel in the platform compared to the original design, which is the whole point of the work. Reducing the diameter of the outer column's top part is efficient at decreasing the objective function but increases also significantly the pitch and surge motions. A smaller D_{OCtop} means less stiffness in pitch and drives ω_5 dangerously close to the wind excitation. For instance, D1 presents unacceptably large pitch and surge motions, even with an unchanged L_{pont}.
Reducing the pontoon length has moderate effects on the maximum response. But the resulting decrease in mass and heave added mass takes ω_3 close to the wave frequencies. Since that degree of freedom is not represented in the linear model, it needs to be monitored through its natural frequency. The 0.32 rad/s constraint on ω_3 mentioned in section 4 would reject D3, D4 and D7.

Design	L_{pont} / D_{OCtop} [m,m]	M_{steel} [kg]	Max surge [m]	Max pitch [deg]	Max M [N.m]	ω_1 [rad/s]	ω_3 [rad/s]	ω_5 [rad/s]	ω_7 [rad/s]
D0	[37 , 13.4]	6.021E+06	31.9	8.143	32.13	0.039	0.223	0.310	4.40
D1	[37 , 9]	5.411E+06	35.4	18.6	42.8	0.041	0.24	0.094	4.47
D2	[37 , 6]			Not stable					
D3	[32 , 13.4]	5.596E+06	32.38	9.6	32.1	0.041	0.33	0.19	4.64
D4	[32 , 15]	5.863E+06	32.05	8.24	34.8	0.040	0.36	0.23	4.60
D5	[32 , 11]	5.241E+06	34.13	14.9	37.34	0.042	0.29	0.125	4.69
D6	[32 , 9]			Not stable					
D7	[30 , 13.4]	5.426E+06	32.7	10.6	32.5	0.041	0.34	0.18	4.75
D8	[40 , 9]	5.666E+06	33.8	14.4	36.4	0.040	0.23	0.115	4.34
D9	[40 , 6]			Not stable					

Table 6: Linear model predictions for different design across the design space

In conclusion, optimizing the platform will go down to how much D_{OCtop} can be decreased before making the system too unstable, and how much L_{pont} can be decreased before having resonance in heave. It must recalled that multiple aspects of the real system's response are not accounted for. Typically, changing the length of the pontoons will affect significantly the bending moment within the legs. The results given here must be therefore analyzed with the model capability and limitations in mind.

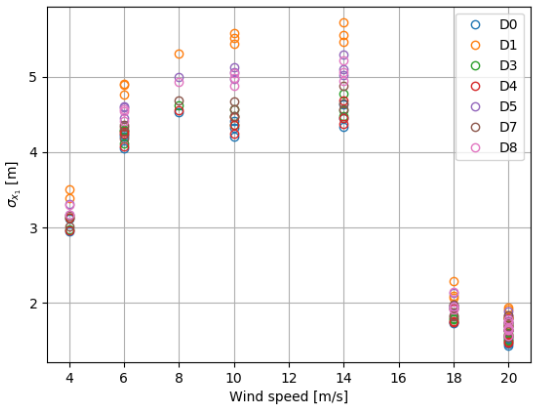

(a) Standard deviation of the surge response

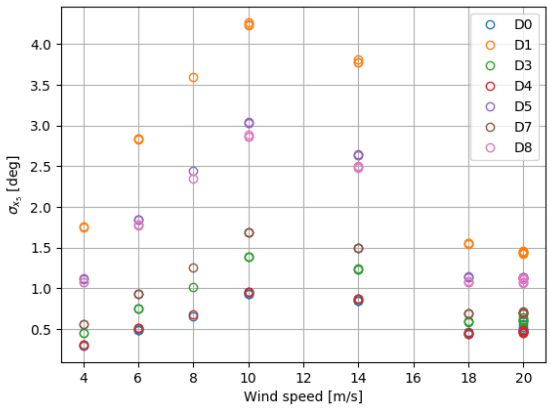

(b) Standard deviation of the pitch response

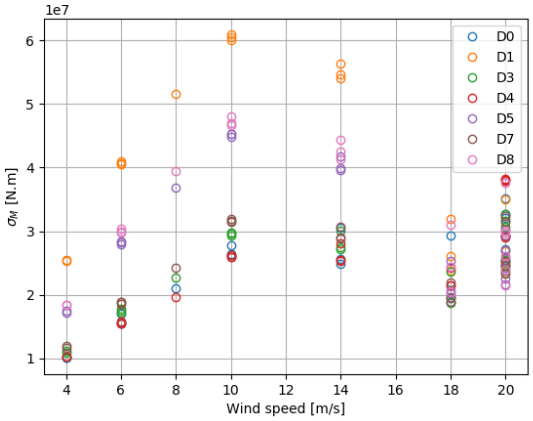

(c) Standard deviation of the tower base bending moment response

Figure 18: Standard deviation of the original design's response to operational sea states

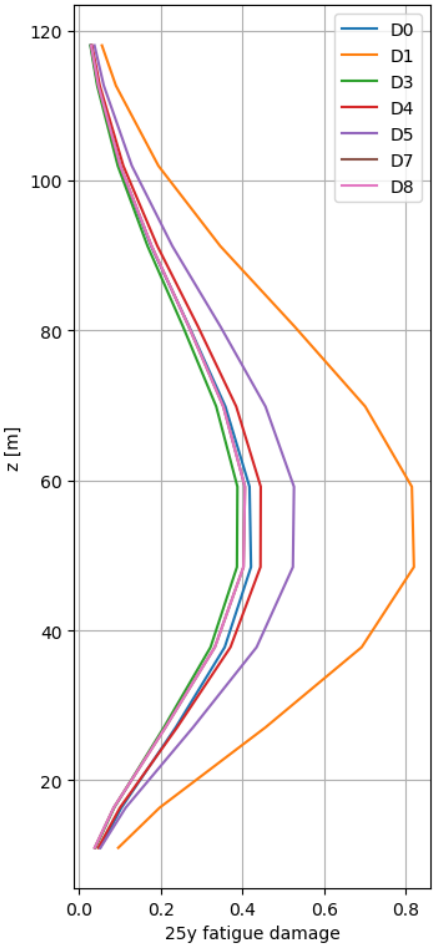

Figure 19: 25-year fatigue damage from tower base to tower top

Conclusion

The present work is an effort towards the development of multi-disciplinary gradient-based optimization of floating wind turbines. It wants to contribute to designing cheap and performant semi-submersible substructures for wind turbines growing in size. The innovation of the project lies in its use of the efficient mathematical methods from gradient-based algorithms, combined with the accurate potential flow calculation for large-volume hull shape.

The main effort of the project was the building of a computationally efficient low-fidelity model of a FWT in the OpenMDAO framework. Using the base geometry of the OOStar and the DTU 10MW turbine, the model solves the linearized equation of motion in the frequency domain for three degrees of freedom, namely surge, pitch and the first tower bending mode. The WADAM solver is called to compute the hydrodynamic coefficients of the hull and the wave excitation forces. Thrust force spectra are used to represent the wind action. The one asset of the model is its full parameterization, coupled with the automation of panel meshing and hydro computation. Changing one of the platform dimensions is thus made very simple. A comparison of the linear results with an integrated SIMA model showed the accuracy range and limitations of the linear model. The response to waves is captured quite well but the limited aerodynamic modeling causes a major underestimation of the pitch response for above-rated wind speeds. This is reflected in the tower fatigue damage, for which the distribution is correct but lower than predicted by SIMA.

A reflection about the key performances of a FWT led to the construction of an optimization problem. In order to reduce the cost of the system, the mass of steel in the platform can be minimized w.r.t two design variables, namely the pontoon length and the outer columns' top diameter. Constraints based on international standards and model-oriented were applied.

The described optimization problem was applied on a very basic structure to practice on a training model. It allowed to familiarize with optimization and to identify the main procedures and hardships of working with an SQP solver in OpenMDAO.

Time was missing to perform the optimization on the real model. However, a manual exploration of the design space identified the main consequences of modifying the design variables. Therefore, no optimum was found but an overview of the design space and a better understanding of how the optimization should perform was obtained.

Finally, some recommendations for further work are to be presented, as there is a lot of potential for improvement. First, the accuracy of the model needs to be improved. Modeling the rotor using e.g. the BEM theory and solving the catenary equations for the mooring can be part of the solution. Secondly, for the optimization to run smoothly, the objective function, design variables and constraints need to be scaled. To make it efficient, a tedious work of providing the missing analytical partial derivatives should be done. It is very likely that the run time of the model can also be improved with smarter coding and handling of variables. Last, the optimization problem can be enlarged. Not only by increasing the number of geometric variables, but also by making the platform flexible, parameterizing the tower or accounting for the turbine control. Including more disciplines in the process is really what gives added value to the optimization.

References

[1] G.F. Clauss and L. Birk. Hydrodynamic shape optimization of large offshore structures. *Applied Ocean Research 18*, 1996.

[2] Y. Park, B.S. Jang, and J. Kim. Hull-form optimization of semi-submersible fpu considering seakeeping capability and structural weight. *Ocean Engineering*, 2015.

[3] M. Karimi, M. Hall, B. Buckham, and C. Crawford. A mutli-objective design optimization approach for floating offshore wind turbine support structures. *Ocean Engineering*, 2017.

[4] K. Chew, K. Tai, E.Y.K. Ng, and M. Muskulus. Optimization of offshore wind turbines support structures using an analytical gradient-based method. *Energy Procedia 80*, 2015.

[5] I. Fylling and P.A. Berthelsen. Windopt - an optimization tool for floating support structures for deep water wind turbines. In *OMAE2011-49985*.

[6] F. Lemmer et al. Optimization of floating offshore wind turbine platforms with a self-tuning controller. In *OMAE2017-62038*.

[7] F. Sandner, D. Schlipf, D. Matha, and P.W. Cheng. Integrated optimization of floating wind turbine systems. In *OMAE2014-24244*.

[8] T. Ashuri et al. Multidisciplinary design optimization of offshore wind turbines for minimum levelized cost of energy. *Renewble Energy 68*, 2014.

[9] J.M Hegseth, E. Bachynski, and J. Martins. Integrated design optimization of spar floating wind turbines. *Marine Structures*, 2020.

[10] Justin S. Gray, John T. Hwang, Joaquim R. R. A. Martins, Kenneth T. Moore, and Bret A. Naylor. Openmdao: An open-source framework for multidisciplinary design, analysis, and optimization. *Structural and Multidisciplinary Optimization*, April 2019.

[11] John Twidell and Gaetano Gandiosi, editors. *Offshore wind power*, chapter 9. 2009.

[12] S. Butterfield, W. Musial, J. Jonkman, and P. Sclavounos. Engineering challenges for floating offshore wind turbines. *Copenhagen offshore wind conference*, October 2005.

[13] J. Jonkman and D. Matha. Dynamics of offshore floating wind turbines - analysis of three concepts. *Wind Energy*, October 2010.

[14] A. Robertson and J. Jonkman. Loads analysis of several offshore floating wind turbine concepts. In *Proceedings of the 21st International Offshore and Polar Engineering Conference*, 2011.

[15] University of Stuttgart. State-of-the-art fowt design practice and guidelines. Technical report, International collaborative project LIFES50+, March 2016.

[16] A. Robertson et al. Summary of conclusions and recommendations drawn from the deepcwind scaled floating offshore wind system test campaign. In *OMAE2013-10817*.

[17] Z. Gao and E. Bachynski. *Integrated dynamic analysis of wind turbines*. Marine technology department at NTNU.

[18] Amy N. Robertson et al. Oc5 project phase ii: validation of global loads of the deepcwind floating semisubmersible wind turbine. In *Energy Procedia 137 (2017)*. EERA DeepWind conference 2017.

[19] M. Kvitten, E. Bachynski, and T. Moan. Effects of hydrodynamic modelling in fully coupled simulations of a semi-submersible wind turbine. In *Energy Procedia 24 (2012)*. DeepWind conference 2012.

[20] University of Stuttgart. Design practice for 10mw+ fowt support structures. Technical report, International collaborative project LIFES50+, April 2019.

[21] University of Stuttgart. Public definition of the two lifes50+ 10mw floater concepts. Technical report, International collaborative project LIFES50+, April 2018.

[22] C. Bak, F. Zahle, R. Bitsche, T. Kim, A. Yde, L.C. Henriksen, P.B. Andersen, A. Natarajan, and M.H. Hansen. Design and performance of a 10mw wind turbine. Technical report, DTU Wind Energy, 2013.

[23] O. Anaya-Lara, J.O. Tande, K. Uhlen, and K. Merz. *Offshore Wind Energy Technology*. Wiley, 2018.

[24] Leon Emry Borgman. Ocean wave simulation for engineering design. *Journal of the Waterways and Harbors Division*, 1969.

[25] DTU. State-of-the-art models for the two lifes50+ 10mw floater concepts. Technical report, International collaborative project LIFES50+, April 2018.

[26] Wind turbines - part 3: Design requirements for offshore wind turbines. Technical report, International Electrotechnical Commission (IEC), 2009.

[27] A. Krieger et al. Design basis. Technical report, Life50+ European collaborative project, 2015.

[28] G. Benveniste et al. Lcoe tool description, technical and environmental impact evaluation procedure. Technical report, Life50+ European collaborative project, 2016.

[29] DNVGL. Floating wind turbine structures. Technical report, DNVGL-ST-0119, 2018.

[30] DNV. Fatigue design of offshore steel structures. Technical report, DNV-RP-C203, 2011.

[31] Turan Dirlik. *Application of computer in fatigue analysis*. PhD thesis, University of Warwick, 1985.

[32] DNVGL. Support structures for wind turbines. Technical report, DNVGL-ST-0126, 2016.

[33] John Marius Hegseth and Erin E. Bachynski. A semi-analytical frequency domain model for efficient design evaluation of spar floating wind turbines. *Marine Structures*, 64, 2019.

[34] O. Faltisen. *Sea loads on ships and offshore structures*. publisher, 1993.

[35] R.C MacCamy and R.A Fuchs. Wave diffraction on piles: a diffraction theory. Tech. memorandum no 69, Beach erosion board - Corps of engineers, 1954.

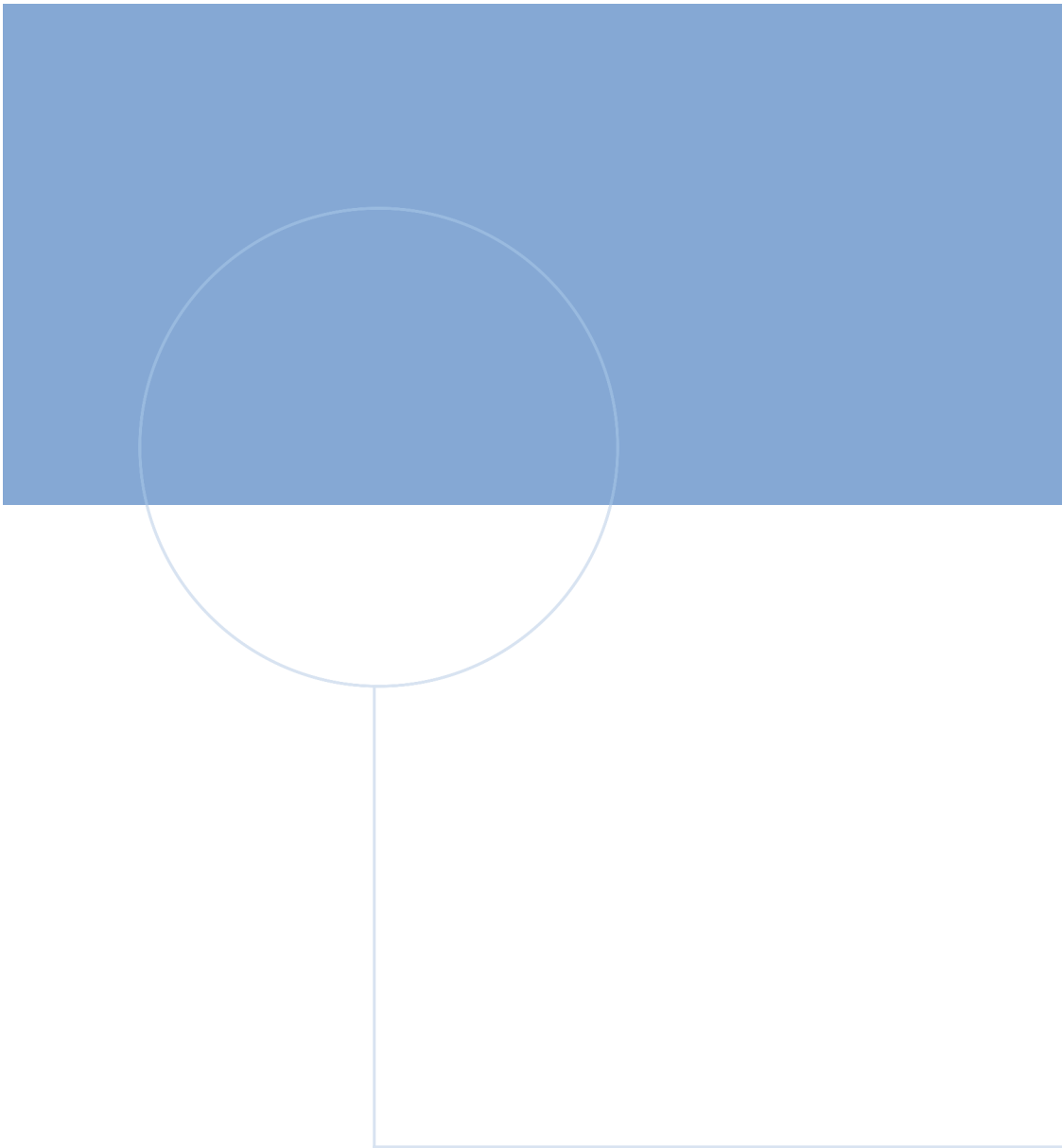

NTNU

Kunnskap for en bedre verden